Corrosion Detection Using Metal Coatings On Fiber Optic Sensors

by

Paul M. Schindler

Thesis submitted to the Faculty of the

Virginia Polytechnic Institute and State University

in partial fulfillment of the requirements for the degree of

MASTER OF SCIENCE

in

Electrical Engineering

APPROVED:

Richard O. Claus, Chairman

Kent A. Murphy

Ira Jacobs

May, 1995

Blacksburg, Virginia

Key Words: Corrosion Detection, Fiber Optics, Sensors, Smart Materials, Interferometric, Gratings

Corrosion Detection Using Metal Coatings On Fiber Optic Sensors

by

Paul M. Schindler

Richard O. Claus, Chairman

Electrical Engineering

Fiber optic sensors have been utilized as corrosion sensors by depositing metal coatings to the surface of the sensors. Three types of fiber optic sensors were investigated as candidates for corrosion detection: the extrinsic Fabry-Perot interferometer (EFPI), the absolute extrinsic Fabry-Perot interferometer (AEFPI), and the long period grating (LPG) fiber optic sensor. The corrosion monitoring technique used with the EFPI and AEFPI sensors exploits the ability of a thick coating of metal to maintain strain information in fiber optic strain sensors. The sensors are placed under tensile stress, and while in the resulting strained position, a thick coating of metal is applied. Due to an increase in the quantity of material, the sensor does not return to its original position upon release, and strain is maintained within the sensor element. As the metal thickness decreases due to corrosion, this residual strain is released, providing the sensing mechanism for corrosion detection. LPG fiber optic sensors have demonstrated their ability as bandstop filters, by coupling the fundamental guided mode to circularly symmetric cladding modes. The cladding modes are extremely lossy due to the fiber jacket and bending along the fiber. Losses at discrete wavelengths can be monitored to determine the onset and progress of metal corrosion. Background theory and experimental results are discussed and reported for EFPI, AEFPI, and LPG fiber optic corrosion sensors. The study is preceded with an overview of different corrosion sensor designs and methods which are used in the area of non-destructive evaluation.

Acknowledgments

I would like to thank my committee chairman and advisor, Dr. Richard O. Claus, for his continuous support throughout my entire M.S. program at the Fiber and Electro•Optics Research Center. His encouragement and positive attitude helped teach me what is important in being a leader. Thanks also to Dr. Kent A. Murphy and Dr. Ira Jacobs, for their help and support in my research.

I am grateful to all the members of FEORC, both graduate and undergraduate, for their generous support and motivation. I would especially like to thank: , whose inspiration as my mentor and camaraderie as a co-worker fueled my success at FEORC; , for his original ideas during this project, his crucial help with metal deposition, and for sharing his unique perspective on life; , for his help with sputtering deposition, and as a true friend; , for supplying and exhaustively explaining LPG sensors, for his assistance while testing the LPG sensors, and for proofreading this thesis; , for providing LPG test data; , for his "towering" support! I would also like to thank for helping with EFPI sensor fabrication.

Many thanks also to all the members of Fiber and Sensor Technologies, Inc., especially for his help with the absolute EFPI system, and , whose master's thesis spawned my original interest in corrosion detection.

My undying gratitude goes to my wife, , for her steadfast love and companionship throughout the years. She truly brings meaning to my life, and for whom all this is

genuinely for. Thanks also to my parents, ; I will forever be indebted to them both for their unending love and generosity.

This work was sponsored by and the NASA Langley Research Center, under grant NAG-1-1292. The majority of the experimental work was performed at the Fiber and Electro•Optics Research Center (FEORC), newly located within the Plantation Road Research Compound, Blacksburg, Virginia.

Dedication

To my father, who has always been my hero. His steadfast devotion to his engineering career, to his wife, and to his entire family has always been an inspiration to me. Without his support, both material and moral, none of my education over these past seven years would have been possible. I can only aspire to be half the father for my future children as he has been for me.

Table of Contents

List of Illustrations

List of Tables

Chapter One - Introduction

Modern society is dependent on many things which are subject to fatigue due to corrosion: buildings, bridges, aircraft, ships, automobiles, etc. As these enter into their third, fourth, or even fifth decade of service, the need for sensing methods to effectively investigate the extent of their corrosion damage becomes critical. In 1980, the estimated cost of corrosion in the United States was 4.2% of the gross national product, or $160 billion, an equivalent per capita cost of approximately $700[1]; much of the aging infrastructure included in that study fifteen years ago is likely to still be in service today. Unfortunately, incidents such as the Aloha Airlines 737 catastrophic fuselage failure must occur before an issue like aging aircraft becomes well known; soon after the 1988 disaster, Congress passed legislation to develop new nondestructive evaluation systems over the next five years. Many steps have been taken since then to reorganize nondestructive evaluation and damage assessment techniques, but many challenges still remain[2]. By offering the public a wide variety of technologies to monitor corrosion, the best technologies can be made available for the profuse number of applications which exist.

1.1 Corrosion Testing and Evaluation

Many different methods exist to monitor corrosion, from simple visual inspection, to state-of-the-art quantitative sensing methods. In the commercial airline industry, the most popular (and not surprisingly, the least expensive) method for determining corrosion damage is visual inspection[3]. Visual inspection can be characterized as simply the examination of a part for pitting, cracking, discoloration, and/or flaking and bubbling of paint or coatings. The principal flaw of visual inspection, though, is that it is essentially subjective in attempting to quantify the amount of corrosion damage. In some cases, this

could provide misleading conclusions. With some types of bridges, a layer of rust helps protect the structure from further corrosion damage, since the corrosion by-product is atmospherically inert. On the other hand, a metal composite material might be unblemished on the surface to visual inspection, while the underlying metal layers are severely weakened from corrosion damage. Also, in the case of most aircraft, areas which are especially sensitive to corrosion damage or critical to the overall structure of the aircraft are not very accommodating to visual inspection; the aircraft must be removed from service and disassembled to reach these vital areas[3]. Instruments such as fiberscopes can be employed in this case, but they are difficult to manipulate in small closed areas, and the image reproduction can sometimes be misleading. Other methods that are used to detect corrosion include electrochemical and electromagnetic sensing, some of which are summarized below.

1.1.1 Simple Corrosion Detection

Since corrosion is both chemical and electrical in nature, certain electrical methods can be utilized to measure its onset. Essentially, corrosion can be envisioned as an electrical circuit, typically modeled by the galvanic cell; the most simple example of a practical galvanic cell is the power production in a battery. Oxidation, or loss of electrons, occurs at the anode of the system, while reduction, or gain of electrons, occurs at the cathode of the system; metal loss occurs at the anode during corrosion, metal gain occurs (in some cases) at the cathode. There can be physical contact between the anode and cathode, or they can be separated by an electrolyte. In both cases, the circuit must be closed for corrosion to take place. In the case of an iron nail in salt water, the cathode and anode take the form of macromolecules of iron which are distributed over the entire surface area of the nail; hence, rust forms uniformly over the surface[4]. Similar to examining the potential, current, and resistivity of a simple battery, these methods can be applied to examine corrosion. Tests can be performed

under controlled potential conditions, controlled current conditions, and at AC frequencies to measure impedance[5]. With some special modifications, a simple galvanic cell can be used as a corrosion coulometer, which measures the ambient corrosion of steel, taking into account debris accumulation (essentially corrosion products) and airborne contaminants[6].

1.1.2 Corrosion Sensor Development

The variety of corrosion sensors is quite vast; each has its own particular strengths and weaknesses for different applications. Methods for inspecting gas, liquid, and solid material pipelines for corrosion include the use of weight-loss coupons, electrical resistance tests, zero-resistance ammetry (ZRA or galvanic measurements), hydrogen-permeation, electrochemical-impedance measurements (EIM), and linear-polarization resistance sensors (LPR)[7]. Additionally, aqueous corrosion detection has been demonstrated through the development of an electrochemical noise sensor. The sensor consists of a voltage source and a current source, with data being evaluated using power-spectrum analysis. The presence of corrosion corresponds to an increase in the amplitude and number of fluctuations of the voltage and current power-spectrum densities. The results of the tests show that current-noise measurements were found to be more comparable to typical methods of corrosion detection than potential-noise measurements[8].

1.1.3 Corrosion Micro- (and Macro-) Sensors

The drive towards the miniaturization of sensors has affected corrosion engineering substantially, with the development of many different types of corrosion microsensors, along with the development of microprocessing technology for faster, remote data manipulation and storage. Different kinds of non-optical corrosion microsensors include single-ion redox transducers, chemically sensitive semiconductor devices, galvanic

transducers, polarization transducers, and resistance transducers, among others. Laboratory tests have been documented on a three-electrode sensor, a current distribution probe, an electrical resistance probe, and a multiple-element sensor[1,9]. Additional microsensors include surface acoustic wave (SAW) devices, and the quartz crystal microbalance (QCM) device[10]. In many areas, such as manufacturing process control, automated corrosion detection has moved beyond the domain of research, and has become commercialized. Case studies are available in many fields, explaining the merits and faults behind such systems as the Onguard™ corrosion monitoring system[11], and automated ultrasonic testing systems, which use ultrasonic technology to examine the corrosion of hidden surfaces. One particular case study delves deeply into the actual method of operation of the particular pieces of equipment used on an oil pipeline in the arctic[12]. Also used to inspect long-distance pipelines are autonomous robots, or "pigs" as they are known, one of which employs 448 sensors around the entire circumference of the forty-eight inch diameter robot. These sensors are used to detect (among other things) dents, cracks, and corrosion damage, all from the inside of the pipeline[13].

1.1.4 Thin-Film Corrosion Detection

X-ray diffraction, a type of thin-film analysis, can be performed to interrogate corrosion, analyzing surface composition and morphology. The surface being interrogated is usually an oxide layer which has formed following exposure to a corrosive medium. X-rays incident on the surface of the specimen scatter according to oxide chemistry, grain size, thickness, and lattice parameters and orientation. For the method to be effective, certain geometrical requirements must be met, dictated mostly by Bragg's law of diffraction. The sample can be measured directly following corrosion, or first ground into a powder[5]. Electron probe microanalysis is similar to x-ray diffraction in that the corroded sample

emits characteristic x-rays when interrogated with high-energy electrons. The difference is that the sample is interrogated over a very small surface area, usually one micron in diameter. This precision gives the test operator the ability to examine very specific areas with greater ease[5]. When elliptically polarized light impinges upon a thin-film surface, the reflected wave will exhibit a change in polarization, which can be correlated to the type and thickness of the thin film. This type of corrosion evaluation is known as ellipsometry. The laws which dictate the reflected wave's characteristic polarization shift are primarily Fresnel's Law and Snell's Law of Refraction[14]. Finally, one novel method for detecting corrosion is a thin-layer activation method for detecting minute losses of material. A section of interest on the sample is radioactivated and calibrated to sensing equipment before corrosion takes place. The change in radioactivity of the active portion is monitored as the thickness is reduced from wear or corrosion. Although the method is very accurate, it is limited to a surface depth of a few hundred microns[15].

1.2 Optical Sensor Methods for Corrosion Detection

The use of optical sensors and fiber optic sensors is quite new in the corrosion detection arena; their popularity has grown recently due to advances in materials and sensing research. Fiber optic sensors have the advantage of small size, low weight, and an inherent immunity to electromagnetic interference. Potentially, they may be multiplexed with other fiber optic sensors, as well as with optical communication systems. Several unique methods for detecting corrosion will be explored, concluding with an overview of the methods explored in this research.

1.2.1 Past Optical Corrosion Sensor Research

One method for detecting the corrosion of metals utilizes a plasmon fiber optic sensor. The theory centers around the premise that, as polarized light propagates through the core of a single mode fiber coated with a thin film of metal, energy is coupled into the metal in the form of surface plasmons, which then changes the intensity of the light exiting the fiber. As the thickness of metal is reduced due to corrosion, the number of surface plasmons is reduced, which is sensed as an increase in intensity[16,17]. While this sensor has shown that it can monitor corrosion, it is somewhat difficult to manufacture, since metal coatings must be applied to the core of the fiber, a relatively delicate process. Other simpler and less accurate intensity-based methods use unpolarized light, and metal coatings on multi-mode fiber; intensity differences are simply a function of how much interference is created by the metal coatings. Another fiber optic method of corrosion detection is the "micromirror" sensor; an optical fiber is coated at one end with a chemically sensitive substance whose index of refraction changes when subjected to corrosion, changing the behavior of the reflected signal[10]. Other optical methods include using holographic interferometry, thermography, and evanescent wave absorption spectroscopy. In holographic interferometry, a transmission hologram is taken of the specimen before corrosion takes place. The subsequent decrease in thickness is seen through the original hologram as an increase in the number of interference fringes. The technique is quite accurate, but very susceptible to changes in material microstructure and position, causing an insurmountable decrease in fringe contrast[18]. Since most types of paints used to protect sheet metals from corrosion are transparent to infrared radiation in the 3.5-5.5 micron range, thermography can be utilized to examine corrosion under a layer of paint. To work effectively, the test samples are regulated at an elevated temperature and must exhibit distinct emissive images during corrosion, versus non-corroded specimens. The technique suffers from subjective analysis, however,

since determination of corrosion is dependent on comparisons to reference photographs[19]. A relatively unique method of corrosion detection uses optical fiber Fourier transform infrared (FT-IR) evanescent wave absorption spectroscopy; the sensing method is based on Attenuated Total Reflectance (ATR) spectroscopy. Qualitative tests were performed on powdered samples of aluminum alloy and aluminum hydroxide (the most common by-product of aluminum corrosion). The fiber sensors are extremely sensitive to very small amounts of sample material, demonstrating that the technique merits more quantitative studies[20].

1.2.2 Thick-Film Coated Strain Sensors for Corrosion Detection

Thick film coatings[a] on fiber optic strain sensors have demonstrated the ability to store strain history of extrinsic Fabry-Perot interferometer (EFPI) sensors[21]. The theory behind this memory storage revolves around inducing plastic deformation of the metal coating encapsulating the interferometric sensor, and the ability of this plastically deformed metal to hold the sensor in the strained position. Since a reduction in the thickness of the plastically deformed metal would cause the sensor to relax to its pre-strained state, this method of memory retention in metal coated strain sensors would be feasible for corrosion detection. However, before the sensors can be used for corrosion detection, plastic deformation of the thick metal coating must first be induced. This plastic deformation can be difficult to achieve, since the process of applying a thick coating of metal is quite involved, and achieving plastic deformation of the metal can sometimes cause the sensor to break; with so much time and effort placed on achieving a thick metal coating, breaking the sensor attempting to induce plastic deformation becomes cost prohibitive.

---

[a] "Thick film coating" is a relative term, used to differentiate it from thin film technology used primarily in the microelectronics field; the coatings used on the all the sensors are between one and fifty microns thick.

The method would work similarly if the sensor were first strained, and while holding the sensor in this strained position, a sufficient amount of metal was applied to the sensor so as to hold the sensor in the strained position; the metal coating would hence be in a state of compression upon release, assuming there is adequate adhesion between the metal coating and the glass fiber. Then, as the volume of metal is reduced due to corrosion, or the strength of the metal is compromised by corrosion, the sensor would relax back to its original pre-strained position. It is the relaxation over the corrosion lifetime of the sensor that is the sensing mechanism of part of the corrosion sensor design in this study.

1.2.3 A New Method of Corrosion Detection

The long period grating (LPG) optical fiber sensor is a technology that has just recently been developed. The LPG sensor responds to changes in the index of refraction surrounding the sensor. The proposed method of corrosion detection is to coat the sensor with metal and examine its response as the metal corrodes and the ambient index of refraction changes.

1.3 Overview

Chapter Two explores the various theoretical aspects of this study, starting with the design of the EFPI and AEFPI systems, followed with the corrosion sensing method for metal coated strain gauges. Some theory behind the LPG sensor is also discussed. Chapter Three details the experimental results of tests performed. First the strain sensor fabrication methods are described, followed with detailed steps on how the metal coatings are achieved. The method of strain storage is explained, along with several interesting obstacles encountered. The corrosion tests and their results are then explored; the chapter concludes with the LPG corrosion sensor test results. Chapter 4, Conclusions, highlights the principal

results for the thesis, and suggests some possible courses of action future work in corrosion detection using fiber optic sensors could take. It should be noted at this point that although most of the recent interest in corrosion detection is focused on aluminum corrosion, this study examines fiber optic sensors coated with copper. The principle reason for this is that copper is much easier to apply in thick coatings on the sensors, due to it's electrically conductive oxide. Aluminum quickly develops an insulating oxide layer, one reason it is used predominantly in the aerospace industry. By demonstrating the fiber optic sensors' ability to successfully monitor the loss of metal coating, it can be maintained that the technology would perform similarly regardless of the type of metal used.

Chapter Two - Theoretical Development

The method of corrosion detection examined in this portion of the study revolves around the ability of a thick metal coating to hold a fiber optic strain sensor suspended in elastic strain. The theoretical mechanics behind this sensing action are dependent on several requirements; however, these conditions are not always necessary and/or sufficient for corrosion sensing to occur. They include:

- Perfect adhesion at the glass/metal interface
- Uniform corrosion over the surface of the sensor
- Uniform corrosion over the lifetime of the sensor
- Metal coating strain behavior equivalent to bulk metal
- Zero strain on the sensor at zero coating thickness

In actual tests, the aforementioned conditions are subject to practical limitations and other physical laws:

- Adhesion between the glass and metal is dependent on which method is used to apply the initial coating of metal.
- Due to variations in environmental surroundings and conditions, and also sensor surface mounting schemes, corrosion could occur more rapidly on different surfaces of the sensor.
- Uniform corrosion over the lifetime of the sensor is very unlikely, due to the reduction in surface area as the coating thickness decreases.
- The physical constants and strain behavior of the relatively thin metal films used in this study are certainly different than those quoted in technical references for bulk metal.

- Because sensor strength is paramount to its success, it becomes necessary to apply a marginal amount of metal before straining occurs, since sensors with metal coatings tend to be stronger.

Theory concerning the operation of the fiber optic strain sensors will be addressed, followed by the theoretical derivation of the strain sensing method. The chapter is concluded with an investigation into the theory behind the LPG sensor and its proposed corrosion monitoring capabilities.

2.1 The Extrinsic Fabry-Perot Interferometer

The extrinsic Fabry-Perot interferometer was initially conceived by Murphy *et al*[22]. A diagram of the sensor and its support system is shown in Figure 2.1. A 1330 nanometer laser diode injects light through single mode silica fiber into a two-by-two fiber coupler. The transmitted light is split between the output ports of a 2x2 bi-directional coupler, as shown in the figure. The light in the lower leg is lost, since this end is shattered, and placed in index matching gel, and therefore does not reflect light. The light propagating in the other output arm interrogates the sensor element. The input fiber of the sensor is cleaved to maximize the amount of reflection at the glass-air interface. Taking the indices of refraction of glass and air into account, the reflection at this interface is approximately four percent. Hence, the majority of the light propagates across the air gap to the second reflector endface, where another four percent is reflected back across the air gap. The reflections other than the aforementioned ones are negligible due to the low reflectivity of the endfaces, and losses in the air gap. Since the two reflected signals are coherent, they interfere and propagate back through the fiber coupler to the photodiode detector head. The observed intensity at the detector is given by

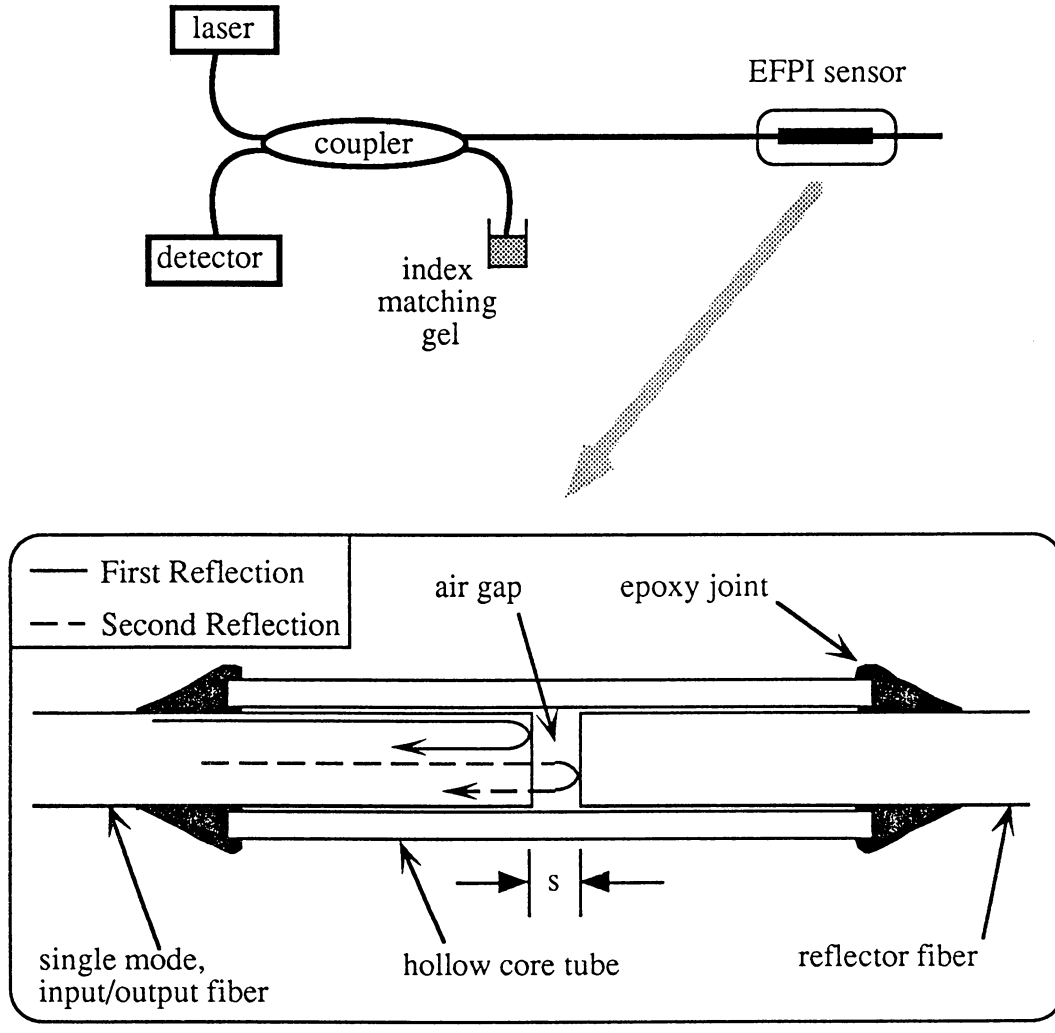

Figure 2.1: EFPI sensor system

$$I_{det} = A^2\left(1 + \frac{2\,ta}{a + 2s\,tan[sin^{-1}(NA)]}cos\left(\frac{4\pi s}{\lambda}\right) + \left\{\frac{ta}{a + 2s\,tan[sin^{-1}(NA)]}\right\}^2\right), \quad (1)$$

where A is the amplitude of the first reflection, t is the transmission coefficient of the air-glass interface, a is the fiber core radius, s is the length of the air gap, λ is the wavelength of operation in free space, and NA is the numerical aperture of the single-mode fiber, given by

$$NA = \sqrt{n_1^2 - n_2^2}, \quad (2)$$

where n_1 and n_2 are the refractive indices of the core and the cladding, respectively. The type of interference between the two reflected signals depends on the dimension of the EFPI air gap; when the length is an odd integral multiple of $\lambda/4$, destructive interference occurs, and an intensity minimum is detected, and when the length of the air gap is a multiple of $\lambda/2$, constructive interference occurs, causing a maximum in detected intensity. Hence, the detected signal is sinusoidal in nature, as shown in Figure 2.2. The exponential decay of the overall magnitude of the waveform is due to the lossy nature of the air gap region.

2.1.1 The "Turn-Around Point" Dilemma

As mentioned in the previous section, the transfer function curve of the EFPI sensor is sinusoidal. If the sensor operating point is located within the linear region of the response curve, the detected output would be most sensitive to minute variations in applied perturbation. Conversely, if the operating point is at a peak or trough of the response curve, then the sensitivity of the sensor is minimum. The principle reason it is desirable to have the sensor's Q-point within the linear region of the output trace, however, is because of the "turn-around point" effect. As an illustration, assume an EFPI sensor is placed in tension, and then released to return to its original position, a typical response curve might

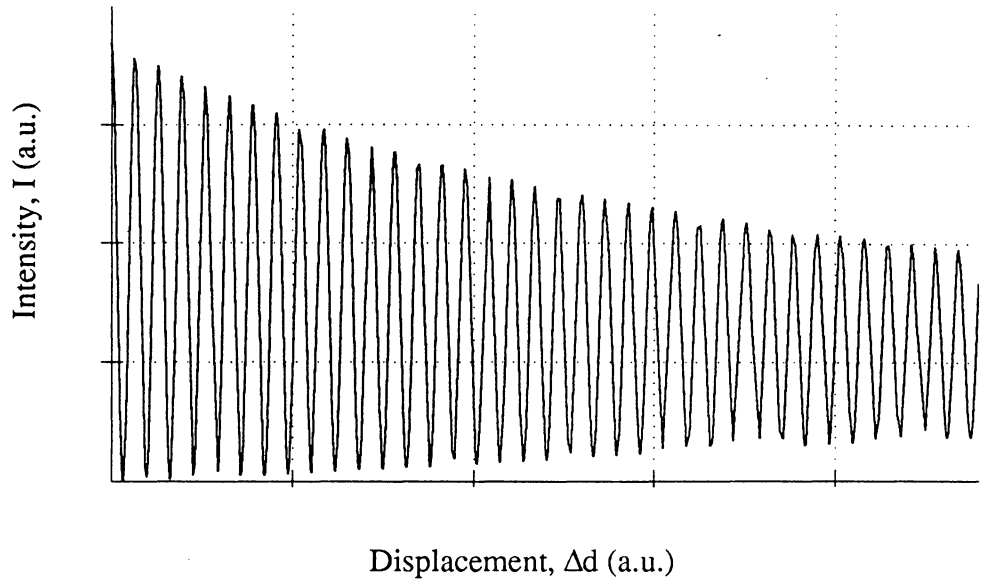

Figure 2.2: Typical EFPI output curve

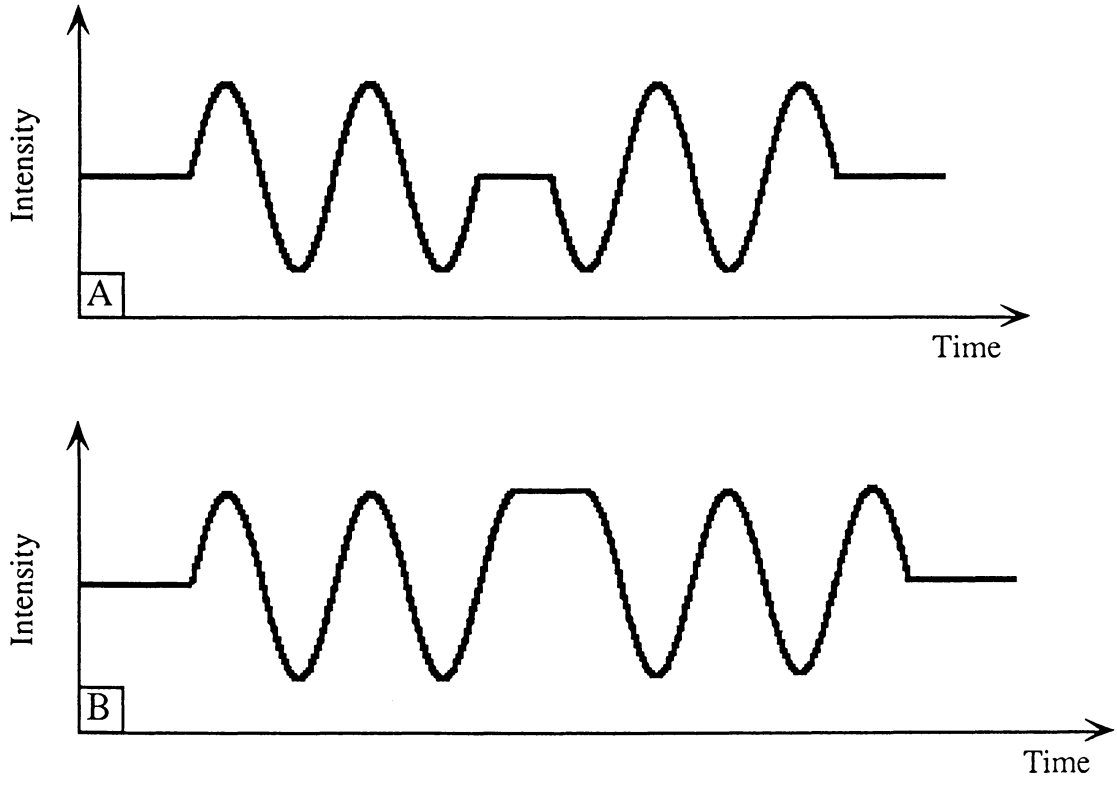

Figure 2.3 (a),(b): Example of ambiguous EFPI output

appear as in Figure 2.3 (a). Notice that the turn-around point is very distinct. However, if the same sensor is strained only one-eighth of the laser wavelength more, the response curve would look like Figure 2.3 (b). In this figure, it is impossible to distinguish the turn-around point; hence it is not clear whether the EFPI sensor has been strained in tension and released, or if the sensor has been strained in tension, held, and strained once again in tension. This turn-around point characteristic is a major limitation of the EFPI system: if the sensor's operating point lies at the peak or trough of the response curve, the sensor behavior becomes ambiguous. Several methods have been developed to alleviate this problem, including interrogating the sensor with two distinct wavelengths, such that the zero-slope region of one wavelength's response curve corresponds to the other's linear region. Another sensing method used in this study is essentially white-light interferometry, to actually measure the dimension of the air gap, known as the absolute extrinsic Fabry-Perot interferometer, or AEFPI.

2.2 The Absolute Extrinsic Fabry-Perot Interferometer

In addition to the elimination of output ambiguity, the AEFPI system offers other benefits. Since the EFPI system requires continuous interrogation of the sensor element, this technology is cost prohibitive for corrosion detection, since the typical lifetime for corrosion sensors would be a minimum of several years; typical laser sources would deteriorate if operated constantly over this time. By utilizing the absolute EFPI system, however, the sensor element can be interrogated and the air gap measured; the system can then be deactivated and reactivated without losing any information during down-time, since the system performs an absolute measurement each time. This type of technology is much more desirable for corrosion detection. A diagram of the AEFPI system used for this study is shown in Figure 2.4. The system resembles the EFPI system shown previously, but

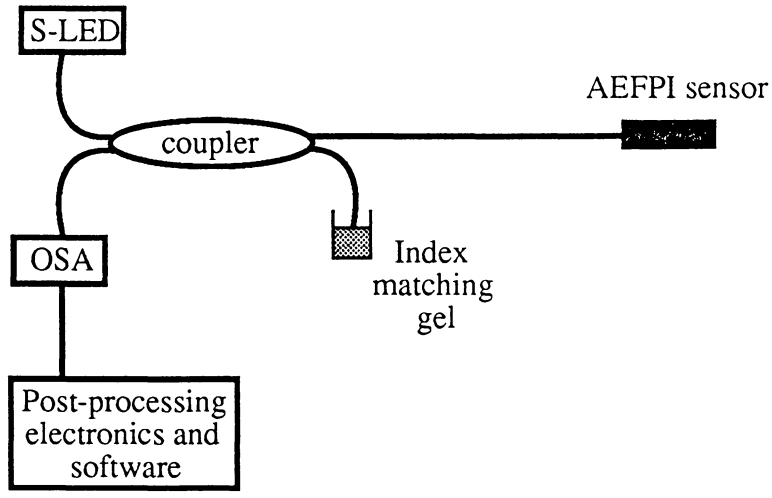

Figure 2.4: Absolute EFPI support system

with several fundamental differences. The sensor element is interrogated with a broadband superluminecent light emitting diode (SLED) source, injecting many wavelengths into the fiber. The sensor element is constructed much like the EFPI, normally with a high-reflectance coating on the reflector fiber; for this study, however, the endface was not coated, since improvements on the computer algorithm used to measure the air gap have been developed. The detector head of the EFPI system is replaced with an optical spectrum analyzer (OSA), which measures the light intensity as a function of the input wavelength. In particular, the phase difference between two particular wavelengths is defined by[23]

$$\Delta\phi = 4\pi s \cdot \left[\frac{1}{\lambda_1} - \frac{1}{\lambda_2}\right]. \tag{3}$$

For a fixed phase difference value of $2\pi n$, where n is a positive integer, equation (3) can be expressed in terms of the gap dimension as

$$s = \frac{n(\lambda_1\lambda_2)}{2(\lambda_1 - \lambda_2)}. \tag{4}$$

For $n=1$, the two wavelengths which are used to calculate the gap dimensions in equation (4) are any two consecutive wavelength peaks from the OSA output signal. Determination of these wavelength peaks is achieved using post-processing computer software, developed by Fiber and Sensor Technologies, Inc[b].

2.3 Corrosion Sensing Method Theory

Restated, the method of corrosion detection investigated in this study revolves around the ability of a thick coating of metal to hold residual strain on a fiber optic strain sensor. As the thickness of the metal coating decreases, the residual strain is released. For theoretical analysis of the corrosion detection mechanics[24,25], the geometry of the EFPI sensor can be

[b] Fiber and Sensor Technologies, Inc., 250 Arbor Drive NE, Christiansburg, VA 24073, 703-382-7556.

simplified as a hollow cylinder of glass, since the sensor architecture used in this study is a sensor design that bonds both the input/output and reflector fiber arms to the hollow core fiber with epoxy; any stress on the sensor is concentrated on the section of hollow core fiber encasing the two single-mode fiber arms. Assuming that there is perfect adhesion at the metal-glass boundary, it follows that the resulting strains are

$$(\varepsilon_x)_{glass} = (\varepsilon_x)_{metal}, \tag{5}$$

that is, the glass hollow core fiber and the metal coating must share the same amount of strain. The force P exerted on the sensor during perturbation can be expressed as

$$P = \int \sigma_x \cdot dA, \tag{6}$$

where σ_x is the axial stress, integrated over the cross-sectional area. The axial stress can be expressed as the strain multiplied by E, the Young's modulus for the material of interest. Hence, for a metal-coated piece of hollow core fiber, the force is expressed as

$$P = \varepsilon \cdot [\pi E_g (r_2^2 - r_1^2) + \pi E_m (r_3^2 - r_2^2)], \tag{7}$$

where r_1, r_2, and r_3 are defined as shown in Figure 2.5. To simplify these equations, the cross-sectional areas for the hollow core fiber and metal coating are denoted as A_g and A_m, respectively, so that equation (7) reduces to

$$P = \varepsilon \cdot (E_g A_g + E_m A_m), \tag{8}$$

or, solving for the strain,

$$\varepsilon = \frac{P}{(E_g A_g + E_m A_m)} \cdot \tag{9}$$

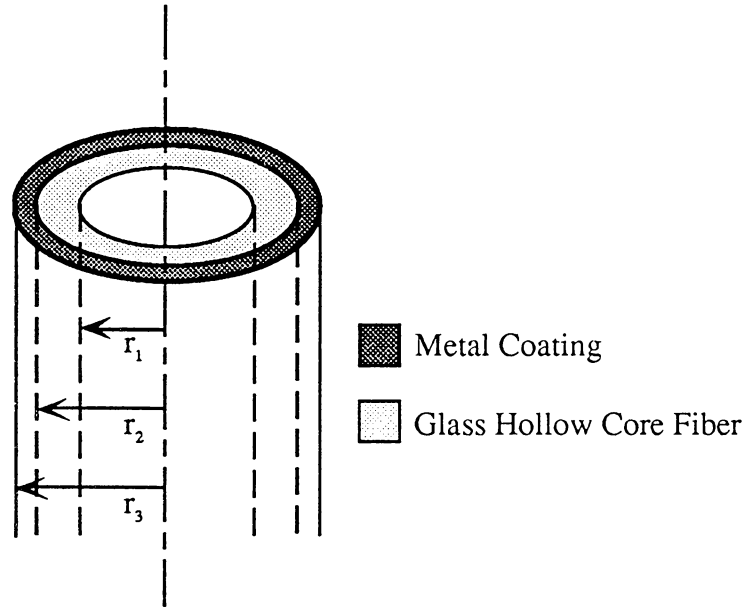

Figure 2.5: Cross-sectional dimensions of metal coated hollow core fiber

Since the assumption holds that there is perfect adhesion between the glass hollow core fiber and the metal coating, and that the strain is constant across the entire length of the hollow core fiber, the strain in each must be the same at all times. This can be expressed as

$$\varepsilon = \frac{P_g}{A_g E_g} = \frac{P_m}{A_m E_m} = \frac{\delta s}{L}. \tag{10}$$

Also shown in equation (10) is the strain equation for the EFPI and AEFPI sensors, where δs is the change in the air gap dimension, and L is the gauge length of the sensor, or the distance between the two epoxy points. Keeping in mind that the sensor is first strained without the metal coating, then the metal is applied, and the strain is then released, the input force before coating can be expressed as

$$P = A_g E_g \cdot \frac{\delta s_{in}}{L}. \tag{11}$$

The sensor gauge length L remains constant throughout the coating and corroding steps, since all of the hollow core fiber is assumed to be coated with metal; the change in air gap before coating is denoted as δs_{in}. Hence, the force on the glass and metal regions are expressed respectively as

$$P_g = \frac{A_g E_g P}{A_g E_g + A_m E_m}, \tag{12}$$

and

$$P_m = \frac{A_m E_m P}{A_g E_g + A_m E_m}. \tag{13}$$

Since the sensor exhibits compressive force instead of tensile force upon release of the stress, the change in the dimension of the sensor's air gap is actually negative; hence, the value for δs_{out} can be conceived as the amount of relaxation upon release of the sensor after applying the metal coating, and is expressed as

$$\delta s_{out} = \frac{P_g L}{A_g E_g} = \frac{P_m L}{A_m E_m}. \tag{14}$$

Using equations (11) through (14), a plot of stored residual strain and change in gap dimension versus metal coating thickness in an EFPI or AEFPI sensor is shown in Figure 2.6, for three different values of δs_{in}. These theoretical curves were derived using a program written in MATLAB®, for several different hollow core fiber pre-strain conditions. The conclusion drawn from this theoretical study is that, assuming there is good adhesion between the hollow core fiber of the sensor and the metal coating, the residual strain release should be sufficient for sensing purposes when the coating thickness is greater than about twenty microns, for either the EFPI or AEFPI sensing methods. A comparison of the theoretical models and experimental data is illustrated in the next chapter.

2.4 Long Period Grating Fiber Optic Sensors

Since the sensing mechanism of the long period grating (LPG) fiber optic sensors is very different than that of either the EFPI or AEFPI sensors, it must be addressed separately. An overview of the fabrication and background theory follows.

2.4.1 Optical Gratings Background

When optical fiber is doped with germanium, it becomes photosensitive; when this germanium doped fiber is exposed to ultraviolet light, there is a change in the index of refraction of the exposed region. When germanium atoms bond with silicon atoms in optical glass (SiO_2), the germanium becomes oxygen-deficient. It is the germanium-oxygen deficiency centers (GODC's) that cause the change in the index of refraction of the UV-exposed glass. The number of GODC's can be increased by hydrogen- or deuterium-loading the fiber, and subsequently making the silica fiber more photosensitive. By

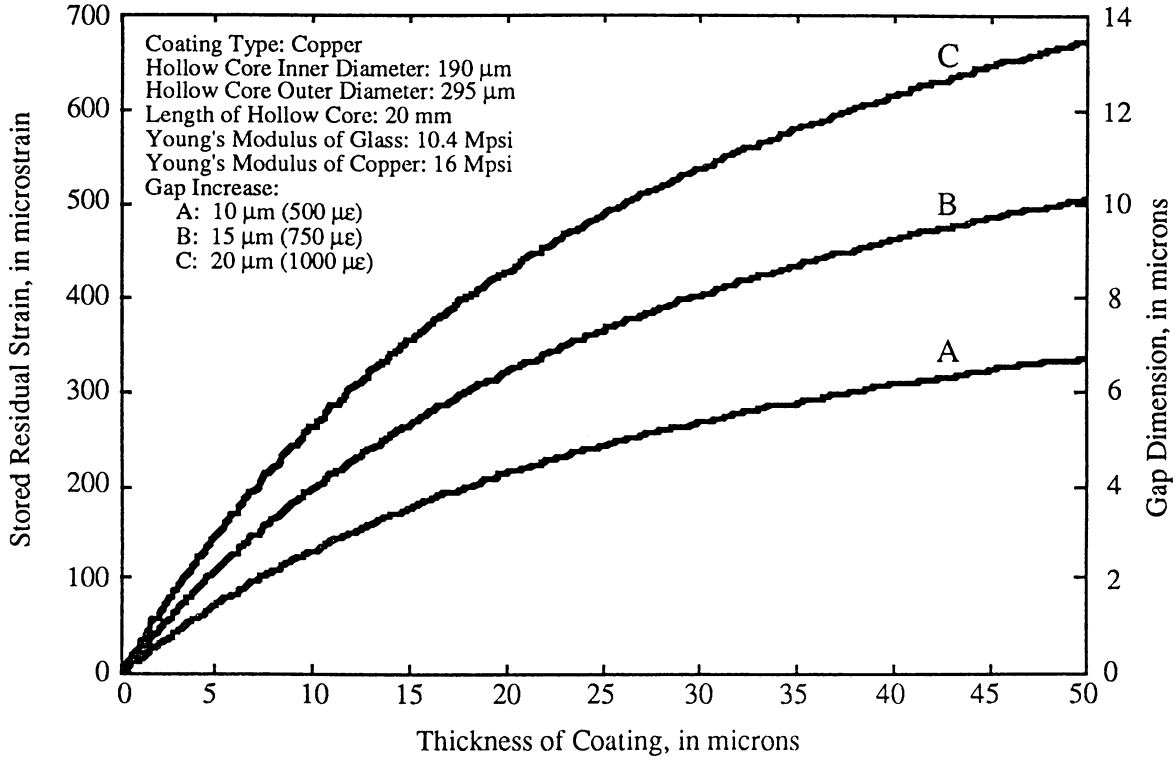

Figure 2.6: Theoretical analysis of corrosion sensing technique

constructing optical fiber with a germanium doped core, and exposing the fiber to 244 nanometer plane-wave light through a mask as shown in Figure 2.7, a periodic change in the index of refraction in the core of the optical fiber is generated, known as a Bragg grating[26]. For a short period grating sensor, the grating periodicity must satisfy the phase matching condition as defined by

$$\Delta\beta = \beta_1 - \beta_2 = \frac{2\pi}{\Lambda}, \tag{15}$$

where β_1 and β_2 are the propagation constants of the fundamental LP_{01} mode, and the reverse fundamental $-LP_{01}$ mode (in the other direction along the fiber), respectively. Keeping in mind that

$$\beta = \frac{2\pi n}{\lambda}, \tag{16}$$

where n is the effective mode index, equation (15) reduces and rearranges to

$$\lambda_R = 2n \cdot \Lambda, \tag{17}$$

where λ_R is the particular wavelength that is reflected from the short period grating. Now consider Figure 2.8, which depicts the different propagation constants of discrete core and cladding modes for a single-mode fiber. The fundamental mode LP_{01} and reverse fundamental mode $-LP_{01}$ have a large propagation constant separation, or $\Delta\beta$, and therefore from equation (15), a short grating period. A long period grating would consequently exhibit a smaller $\Delta\beta$; instead of coupling light into the reverse fundamental mode, light would be coupled into the cladding modes, either in the forward or reverse direction. Since both guided and cladding modes possess discrete propagation constants, a highly wavelength-selective device is obtained. Table 1 has been included to outline the major differences between short and long period gratings.

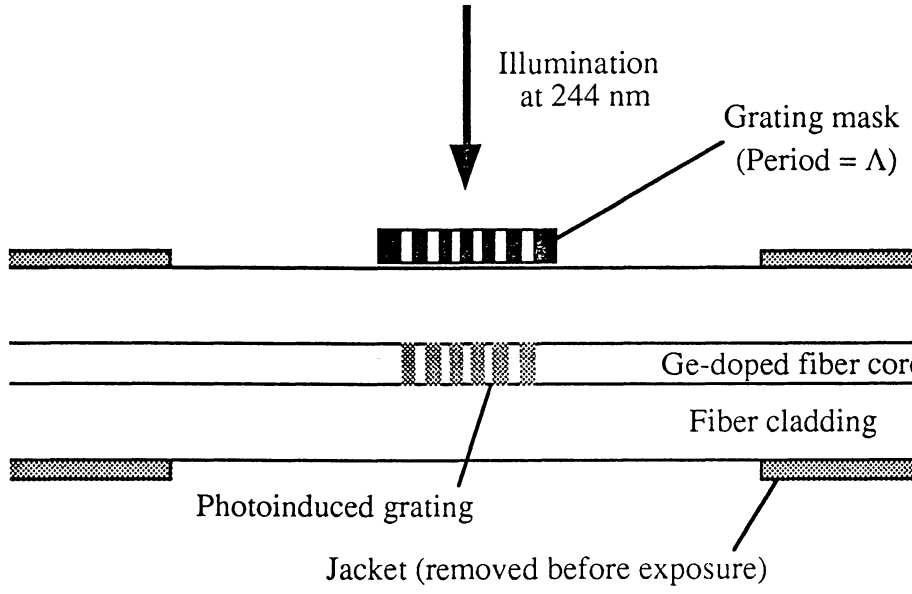

Figure 2.7: Long period grating sensor fabrication

Table 1: Comparison between short period gratings and long period gratings

	Short Period Gratings	Long Period Gratings
Grating period	0.5 - 1.0 μm	100 - 500 μm
3 dB bandwidth of reflected/attenuated wavelength	≈ 1 nm	≈ 10 nm
Back-reflections?	Yes	Negligible

2.4.2 LPG for corrosion sensing

Because long period gratings exhibit negligible back reflections, they are especially attractive in the field of telecommunications. Since it is inherently easier to record longer period gratings, and no advantage is attained from coupling to the reverse cladding modes versus the forward cladding modes, LPG fiber optic sensors are fabricated to couple wavelengths to the forward cladding modes, as shown in Figure 2.8. When these wavelengths become coupled into the cladding modes, they are severely attenuated, due to fiber bending and jacket losses; as a result, an LPG fiber sensor behaves as a wavelength-selective bandstop filter. Because the spectral location of the attenuation bands is dependent on the cladding of the fiber, any index of refraction changes made to the cladding or jacket regions causes a shift in the attenuated wavelengths[27,28]. This wavelength shift is the basis of the sensing mechanics used in this study; an applied coating of metal on the outside of the LPG fiber sensor causes a shift in the attenuated wavelengths within the cladding. As corrosion occurs, a change in the index of refraction will cause the attenuated wavelengths to shift back.

Figure 2.9 shows normalized frequency versus normalized propagation constant for several LP_{lm} core modes[29]. The normalized propagation constant is defined as

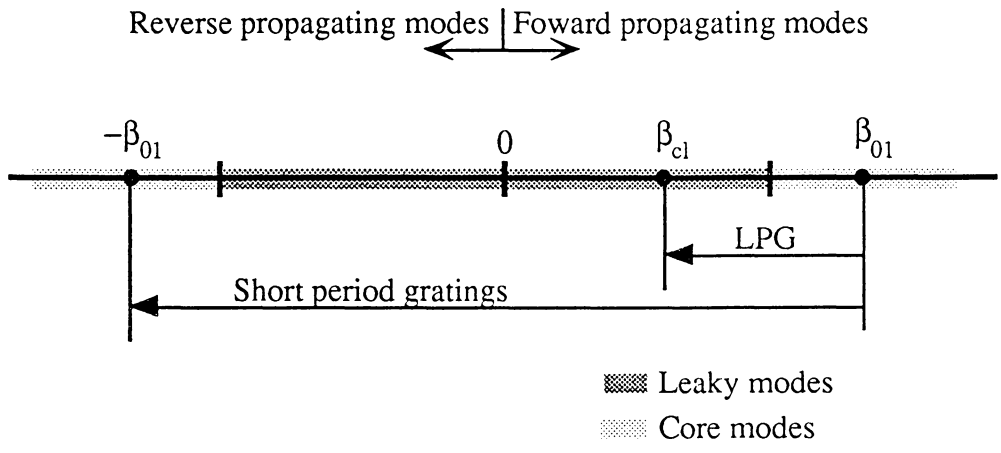

Figure 2.8: Conceptual propagation constant line for grating fabrication

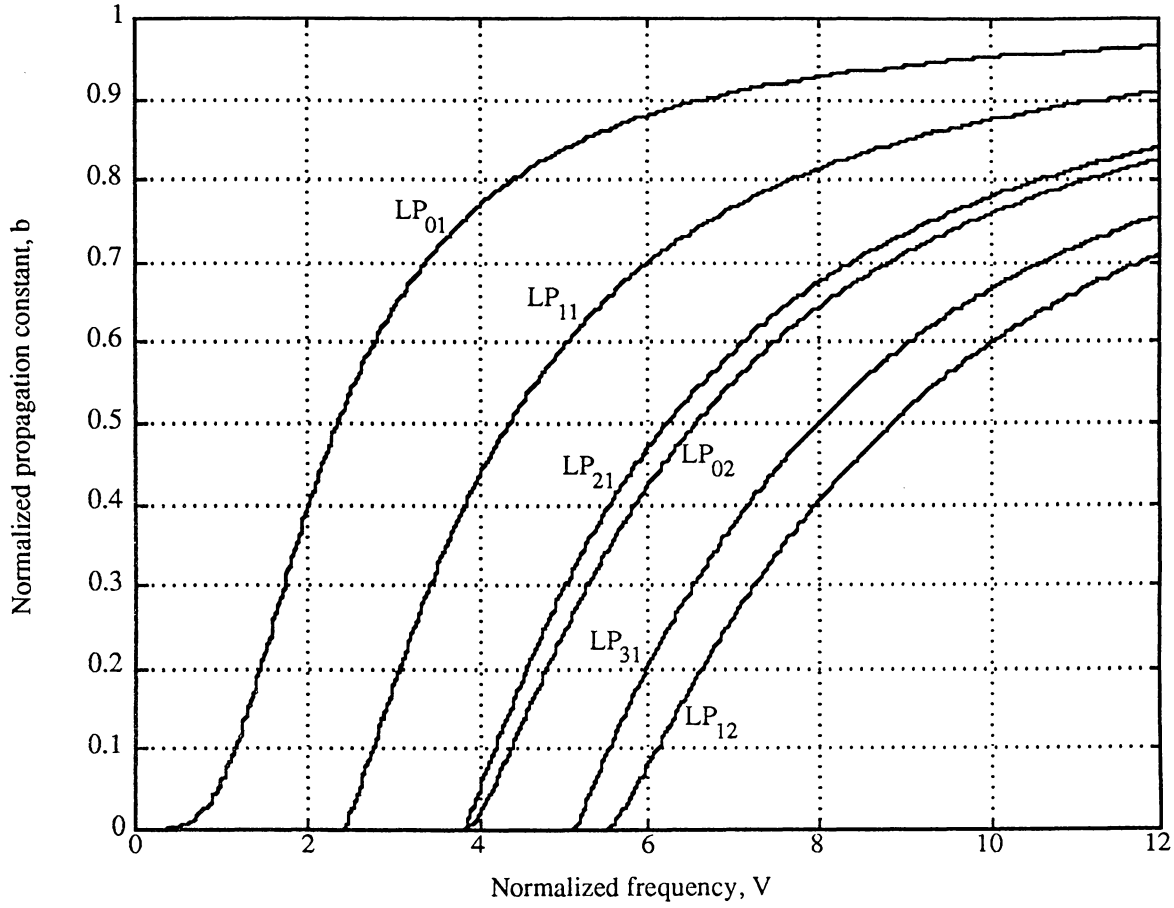

Figure 2.9: Normalized propagation constant vs. normalized frequency

$$b = \frac{\left[\frac{\beta}{k} - n_2\right]}{n_1 - n_2}, \tag{18}$$

where k is the free space propagation constant, and the normalized frequency is defined as

$$V = \frac{2\pi}{\lambda} \cdot an_1\sqrt{2\Delta}, \tag{19}$$

where a is the core radius, and

$$\Delta = \frac{n_1^2 - n_2^2}{2n_1^2} \approx \frac{n_1 - n_2}{n_1}. \tag{20}$$

When β/k equals n_2 (at the cladding), $b=0$, and when β/k equals n_1 (at the core), $b=1$. For our studies, only the LP_{01} mode is of interest. Hence, as wavelength increases (or normalized frequency decreases), the LP_{01} mode approaches the cladding. Restated, the longer wavelengths are coupled into the cladding more readily than the shorter wavelengths, for a given change in cladding properties. Hence, it can be predicted that there should be a greater shift in longer attenuated wavelengths than in shorter ones, for a given change in the medium surrounding the cladding region of the sensor. A similar set of curves exist for the cladding/jacket modes. The only difference in their derivation is that n_1 and n_2, the indices of refraction of the core and cladding, become n_2 and n_3, the indices of refraction for the cladding and jacket, or surrounding medium. Hence, the normalized frequency is defined as

$$V = \frac{2\pi}{\lambda} \cdot dn2\sqrt{2\Delta}, \tag{21}$$

where

$$\Delta = \frac{n_2^2 - n_3^2}{2n_2^2} \approx \frac{n_2 - n_3}{n_2}, \tag{22}$$

and d is the radius of the cladding region. Thus any change in d, n_2 or n_3 causes the V-number, and hence b for the cladding modes to change; the wavelength-selective mode coupling occurs at a different wavelength and a change in the output spectrum is observed. If this shift in the attenuation bands can be measured, the external perturbation can be

quantified. Hence, long period gratings provide a sensing mechanism whereby surface effects like corrosion can be monitored without pre-straining.

Chapter Three - Experimental Results

3.1 Strain Sensor Fabrication

A schematic of the extrinsic Fabry-Perot interferometer and absolute EFPI sensor[c] is shown in Figure 2.1. The type of optical fiber used in its construction is 1300 nm-wavelength, single mode, polyimide-coated fused silica quartz fiber, with a core diameter of 9 microns, a cladding diameter of 125 microns, and a coating thickness of 15 microns. The hollow core fiber is also polyimide-coated fused silica quartz, with an inner diameter of 190 microns, and an outer diameter of 295 microns. To construct the sensors, a fabrication station was implemented, consisting of a microscope mounted above two fiber clamps, one of which was stationary, the other mounted on a three-axis micropositioner. The polyimide coating on the hollow core fiber was first removed using a razor blade, and cleaned with isopropyl alcohol. The end was hand-cleaved to achieve a relatively flat surface into which the fiber is fed. The hollow core fiber is locked in the stationary clamp. The single mode fiber is then stripped of its polyimide coating by burning it first with a lighter flame, and cleaning off the black residue with alcohol. The end is then cleaved using a commercially available fiber cleaver, to achieve an extremely flat endface, maximizing the amount of reflected light. The single mode fiber is cleaved in a manner so that the resulting two endfaces are both used in the sensor. Both fibers are fed into the hollow core fiber. If the sensor is to be used as an EFPI, the gap is set at approximately fifty microns. Knowledge of the exact dimension is not crucial, since the EFPI sensor measures relative strain; if the gap does not exceed half of the coherence length of the laser diode, the sensor will operate successfully. If the sensor is to be used as an AEFPI, however, the gap is adjusted actively, by connecting the sensor to the absolute support system. A gap of ninety microns is ideal for the absolute system, since

[c] Since the principal difference between the two technologies is the method of interrogating the sensors, and not their physical structure, fabrication of both will be addressed simultaneously.

this gives several wavelength peaks which the system relies on to measure the gap dimension. Once the gap is set, epoxy is placed on the fibers, but is not wicked in as before; this would change the set gap, and also tends to pressurize the air inside the hollow core fiber, sometimes creating an air bubble in the glue joint and weakening the epoxy bond. The epoxy is again heated at 60 °C, until it has set; the sensor is then left in a desiccating chamber overnight, to allow the epoxy to completely cure.

3.2 Application of Metal Coating

Because the sensing mechanism in this study requires that a relatively thick coating of copper is applied to hold residual strain in the EFPI or AEFPI sensor, several steps must be performed to apply a sufficient amount of metal. To ensure good adhesion to the glass hollow core fiber, sputtering or evaporation is employed to apply a thin initial coating of metal. Following either of these steps, electroplating is then utilized to apply thicker coatings. During the sputtering or evaporation phases, the sensors are not fixed in the strained position; it is only after either of these steps that any strain is applied. This is for several reasons:

- The sensors are easier to mount in the sputtering or evaporation chambers if they are free from strain.
- The risk of changing the incident strain on the sensors during transportation is eliminated.
- The risk of breaking the sensors is minimized.
- The sensors increase in strength following the application of a thin film of metal, allowing more pre-strain to be applied before electroplating.

This last point proved to be the most pertinent, since an attempt was made early in the study to pre-strain uncoated sensors, with catastrophic results. An overview of the sputtering and evaporation processes follows.

3.2.1 Physical Sputtering

Physical sputtering produces thin films of deposited metal with superior adhesion, compared to those obtained by evaporation or electroplating. The type of sputtering done for this research was performed in a radio frequency (RF) magnetron sputtering chamber. To apply thin coatings of metal, the sensors are either suspended one at a time in the chamber, or mounted on the stainless steel rack[d] with polyimide tape. In either set-up, the sensors are placed between a target and a source gun. The target consists of the metal to be deposited on the substrate, the source gun functions as an electrode. The chamber is then evacuated, and back-filled with argon at approximately 10 millitorr. Argon is used due to its inert properties, and for its relatively large molecular size. The target and source gun are then connected to an RF voltage, and the argon gas is excited to the plasma state. The principle of sputtering is that, as the argon atoms bombard the target with a high amount of energy, atoms of the target material are dislodged off the surface, and accelerate towards the source gun. In the process, some molecules strike the substrate and adhere to the surface. The purpose of using an RF source is that, at frequencies above 10 MHz, the highly mobile electrons in the plasma are able to reach the anode, and hence become grounded, while the less mobile argon ions remain in the plasma. The end result is a nearly-continuous stream of argon ions bombarding the target[30].

[d] The rack was originally designed to hold the sensors during the straining phase; it will be discussed later.

When the sensors were sputtered individually, the resulting thin film of copper was relatively free of oxide. Because the time to evacuate the system and sputter is quite lengthy, however, most of the sensors for this test were sputtered as a group on the stainless steel rack. To increase the spread of the sputtering gun, the chamber must be maintained at a higher vacuum. Unfortunately, when this was done, the amount of oxide deposited on the sensors increased; it is unknown what caused this increase in oxide deposition. As a result, some sensors were lost in attempting to coat copper over the oxide, since oxide layers contain much more surface stress than metal; upon contact with the plating solution, the oxide coating ruptured off of the surface of the sensor. For the latter tests, evaporation was used instead of sputtering.

3.2.2 Thermal Evaporation

The thermal evaporation process is simpler than sputtering, being both quicker and less expensive; the applied coatings are also traditionally thicker than those done using the sputtering process, although this attribute does not particularly impact this study. Even though the evaporation process does not provide the superior adhesion properties as sputtering, it was determined empirically that the amount of adhesion was sufficient for this study. The principal reason is that the entire sensor becomes encapsulated by the metal coating, helping to hold the residual strain on the hollow core fiber. The target sensors are suspended in a vacuum bell jar as shown in Figure 3.1, with a tungsten holder, or boat, underneath them attached to high voltage electrodes. The chamber is filled with oxygen at a pressure of about 20 millitorr, and a plasma is ignited through the entire chamber, known as glow discharge cleaning. This helps to clean the substrate sensors, by heating the surface, and by breaking up surface hydrocarbons much like in sputtering. The chamber is then evacuated to a pressure of 5×10^{-5} torr or lower, to reduce the amount of deposited oxide.

The tungsten boat is heated by supplying a high voltage to the electrodes; the copper melts and evaporates at room temperature, due to the lower operating vapor pressure, and is deposited on the suspended sensors. The support on which the sensors are attached is rotated, to apply an even coating over the entire surface of the sensors. A deposition rate of 22 Å is maintained, at a deposition distance of approximately fourteen inches. Upon removal from the bell jar, the sensors have a bright, clean looking surface; there was no evidence that the coating was heavily oxidized. However, because the coating is extremely thin, care must be taken to quickly apply a thicker coating of copper through electroplating, to avoid any build-up of a more resistive oxide layer.

3.2.3 Electroplating Deposition

To apply thicker coatings of metal, electroplating is the method of choice in metallurgy. The primary requirement for electroplating, however, is that the substrate be electrically conductive. Not only does evaporation and sputtering fulfill this requirement, but the adhesion characteristics of both are reliable. The electroplating process operates much like a conventional wet-cell battery, such as those in automobiles. The plating solution consists of the following ingredients:

- Copper sulfate ($CuSO_4$), 240 grams per liter
- Sulfuric acid (H_2SO_4), 15 grams per liter
- Thiourea, 0.001 grams per liter (used as a grain refiner, to decrease metal grain porosity, by forcing the grains to grow parallel to the substrate)
- Wetting agent, 0.1 grams per liter (used to maximize coverage of substrate, can be substituted with Ivory® dishwashing liquid)
- Brightener, 1 milliliter per liter (also a grain refiner, can be substituted with black strap molasses)

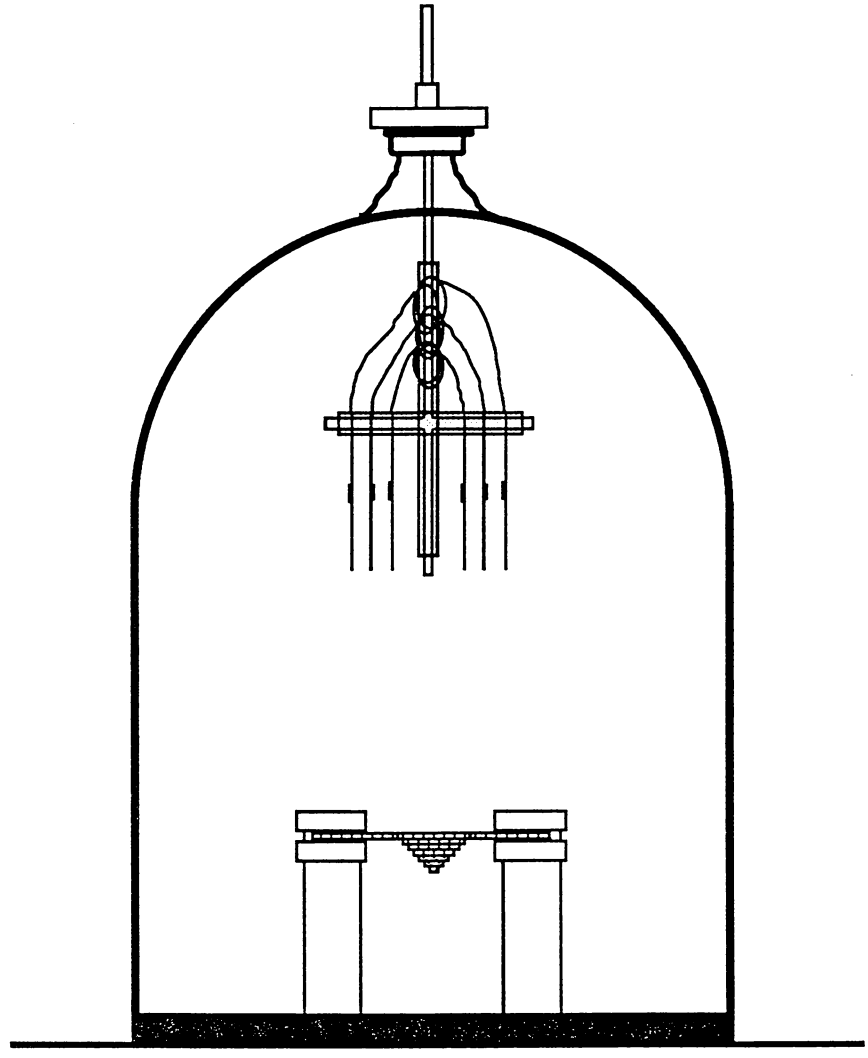

Figure 3.1: Thermal evaporation setup

The setup for electroplating is shown in Figure 3.2. A piece of high-purity copper (A) is placed into the plating solution and is attached to the anode of a current-controlled power supply (B). The cathode is connected to the substrate, in this case the copper coated sensor (C), and is immersed in the solution. Solid contaminants are removed from the solution using a filtration system (D) much like those found in household fish tanks. The solution agitation is maintained using a magnetic stirrer (E). The plating solution acts as an electrolyte, closing the circuit. Positive copper ions in the plating solution are attracted to the negatively charged substrate, adhering to the surface. Several variables affect the adhesion, grain size, and rate of deposition of the plated copper: (1) the current density supported by the substrate, (2) the composition and concentration of the plating solution, (3) the relative location of the sensors with respect to themselves and the anode, and (4) the conductivity of the metal coating on the sensors. Because the exposed surface area of the sensors is very small, the applied current must be maintained at a relatively low level; should it becomes too high, there would be a reduction in adhesion and overall quality. However, if the current density is not maintained above a certain level, the sensors will not be sufficiently negatively charged, and the thin coatings will dissolve into the plating solution. The amount of applied current was generally between twenty and forty millamperes depending on the amount of exposed, activated copper. Also, if a sensor is too close to other sensors during electroplating, electromagnetic field lines emanating from the sensors can cause cathodic shielding, and as a result, uneven copper deposition.

3.3 Application of Stress

Before the sensors are mounted on the stainless steel rack used to apply stress, the sensors are connected to the cathode of the plating system, and a thin coating of copper is applied. This is done to ensure a low-oxide, low-resistance layer of copper is present, before the

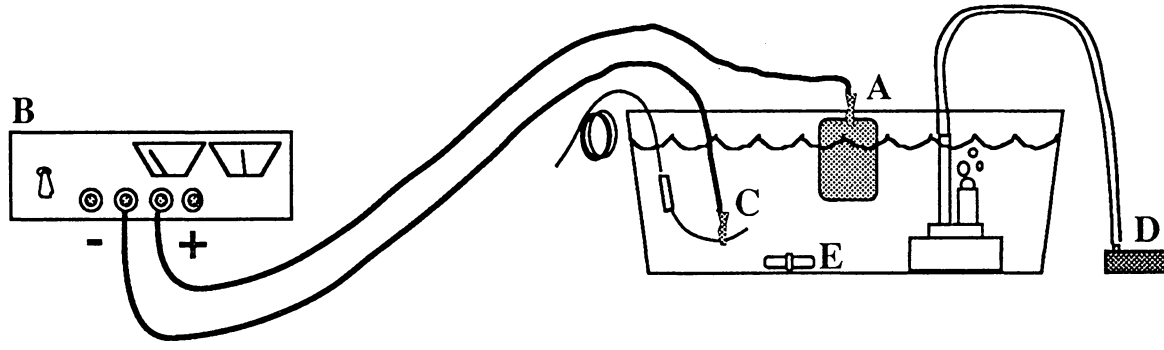

Figure 3.2: Electroplating setup

effort is made to mount and strain them. One reason copper was used in this study is because copper oxide is still conductive, unlike other materials such as aluminum. Due to high oxide surface stresses, applying a thin coating of copper ensures that the first layer of copper remains intact during the plating process, as discussed earlier.

After the sensors have a plated copper coating of about two microns in thickness, they are mounted onto the stainless steel rack. This procedure is the most significant one in attaining functional corrosion sensors, and also the one that required the most re-design throughout this research. The setup for this straining step is illustrated in Figure 3.3. MS-907 epoxy (A) is used to adhere the sensor (B) to the stainless steel rack (C). Once completely hardened, the sensors are stressed by moving the sliding member (D) up with a stainless steel nut (E). An additional nut (F) is used to lock the moving member in place. The sensors are electrically connected to the rack with silver colloidal suspension (G). It was discovered empirically that the copper does not adhere well to the epoxy joints at each end of the sensor. This lack of adhesion posed the problem that, if all the copper separates from these epoxy joints, the electrical connection between the rack and the hollow core fiber of the sensor is interrupted, not allowing plating to proceed. Also, if the sensor epoxy joints are only partially covered with copper, these small connections must support a higher current density, making them susceptible to burning. To alleviate this problem, silver paint was also applied to the epoxy joints of the sensor, and all the exposed fiber up to the stainless steel rack, on both sides of the sensor, to ensure that good electrical contact was maintained. The entire rack was electrically connected to the plating system through a wire connection (H), and the lead-out fibers were protected from accidental detachment by fastening them to the rack with polyimide tape (J). Since the entire rack is electrically connected to the cathode, upon immersion into the plating solution, copper would begin to

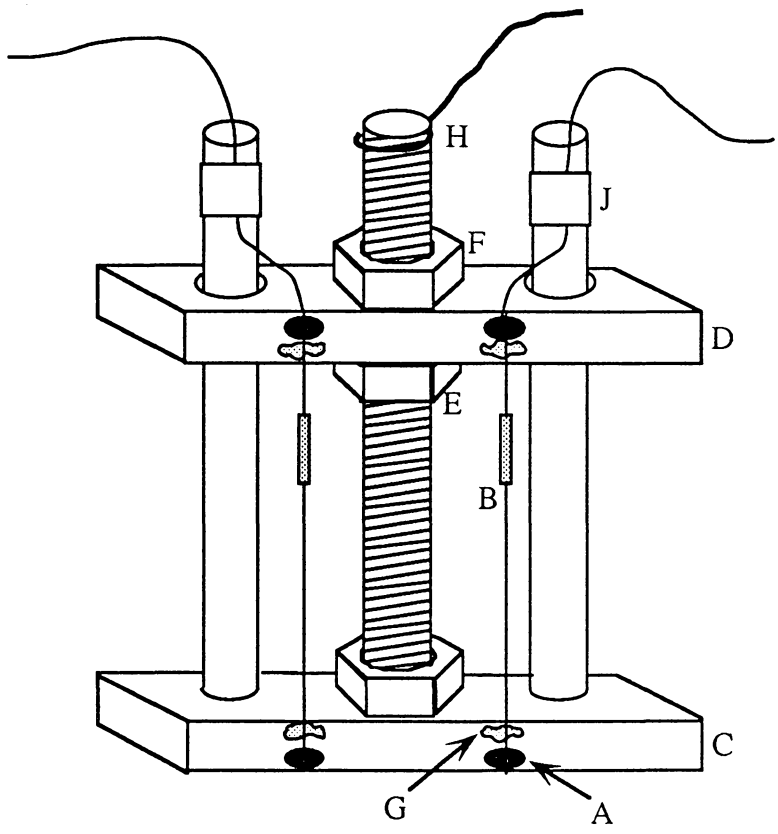

Figure 3.3: Stainless steel straining rack

plate onto the stainless steel rack, as well as the sensors. This would deplete the supply of copper in the plating bath very quickly. To prevent this from happening, the entire rack (except for the sensors) was painted with a thick coating of plating protection liquid, commercially available as StopOff®. This protection liquid behaves much like nail polish; it dries very quickly, and will dissolve in acetone. (It is even bright red in color!) Its principal trait is that it remains inert in most acids, does not contaminate the plating solution, and acts as an electrical insulator.

3.3.1 Adhesion: The Limiting Factor

The governing constituent in determining the final thickness of the electroplated copper, and hence the amount of stored strain in the sensor, was the MS-907 epoxy used to bond the sensors to the rack, and its ability to maintain good adhesion throughout the entire plating phase. Several steps were taken to aid in this adhesion:

- The surface of the stainless steel rack where the fiber was mounted was first roughened with a razor blade, and then cleaned with isopropyl alcohol.
- The bead of epoxy was rather large compared to the size of the fiber, approximately one centimeter in diameter, to increase the surface area of epoxy on the rack.
- The sensor fiber was secured onto the rack with a small piece of tape, to immobilize the fiber during the epoxy cure.
- Another sacrificial piece of optical fiber was placed underneath the sensor fiber, to raise the fiber up and ensure that the entire surface of the sensor fiber was encapsulated in the MS-907 epoxy. This was in lieu of having the sensor fiber rest on the surface of the rack during the cure, and not allowing the fiber to be completely covered in epoxy.

- After the epoxy was completely cured, the entire bead was painted over with a thick coating of StopOff®, to help isolate the epoxy from the plating bath; long period exposure to sulfuric acid is known to compromise the adhesion properties of MS-907 epoxy[31].

These additional measures were partially successful; however, over a twenty-four-hour period in the plating bath, the strain decreased from an approximately 0.1% before immersion into the bath, to almost no strain upon removal from the bath. The results of this loss of adhesion will be presented later.

3.4 Corrosion of Metal Coated Strain Sensors

For the purpose of this study, corrosion is characterized as a decrease in the volume of metal. While this could be interpreted as a somewhat naïve definition, it is sufficient for the scope of this study. Unfortunately, due to time constraints, the corrosion could not be modeled using more typical means, such as long-term salt spray atmospheric tests. Instead, the sensor's metal coating was removed at a constant rate over approximately one hour (depending on the test) using a corrosion medium consisting of a mixture of 10% nitric acid, 20% acetic acid, and 70% phosphoric acid. This mixture was used for its ability to give a very even rate of corrosion; it is typically used in the electroplating industry as a brightening agent.

3.4.1 Determination of Sensor Corrosion Rate

The corrosion rate was determined empirically, by generating a thickness-versus-time curve for several types of corrosion situations. These curves were used along with the known beginning thickness of metal coating on the sensor element to determine the corrosion rate for each sensor test. The corrosion rate curves were developed by first coating a piece of

hollow core with copper. The coated hollow core was then placed in the corrosion bath for a set amount of time, removed, and rinsed off with de-ionized water; the thickness of copper was then measured using a laser micrometer, since mechanical micrometers have a tendency to break the hollow core. These steps were performed in three different tests; the first on a piece of unstrained coated hollow core fiber, the second on a piece of hollow core fiber that was placed under strain during electroplating, and the third on a piece of hollow core fiber under strain, in a 30% agitated solution[e]. The corrosion rate curves are shown in Figure 3.4. As expected, the corrosion rate increased for the situations in which the hollow core was strained, as well as for an agitated situation. In most of the corrosion tests performed on the sensors, the corrosion solution was agitated at 10% to prevent the sensor from being perturbed. During each test, the sensor was immersed completely in the solution, and testing continued until all the copper was removed from the surface, usually within two hours, depending on the initial thickness of copper.

3.4.2 EFPI Corrosion Sensor Test Results

A total of ten EFPI sensors were tested, all of which had been held in stress during the electroplating process. Although final results exist for ten sensors, approximately thirty sensors were fabricated to be subjects in this corrosion study; however, ten of these could not be used due to design flaws, and about ten more failed either during the straining or coating phase. What follows is a synopsis of the test results for the ten EFPI sensors that survived.

The first three sensors were tested, and a written description of the output trace was recorded as the tests progressed. In actuality, there were originally four sensors which were

[e] Liquid agitation was accomplished using a spinbar® permanent magnet stirrer and stir plate, set on 30%.

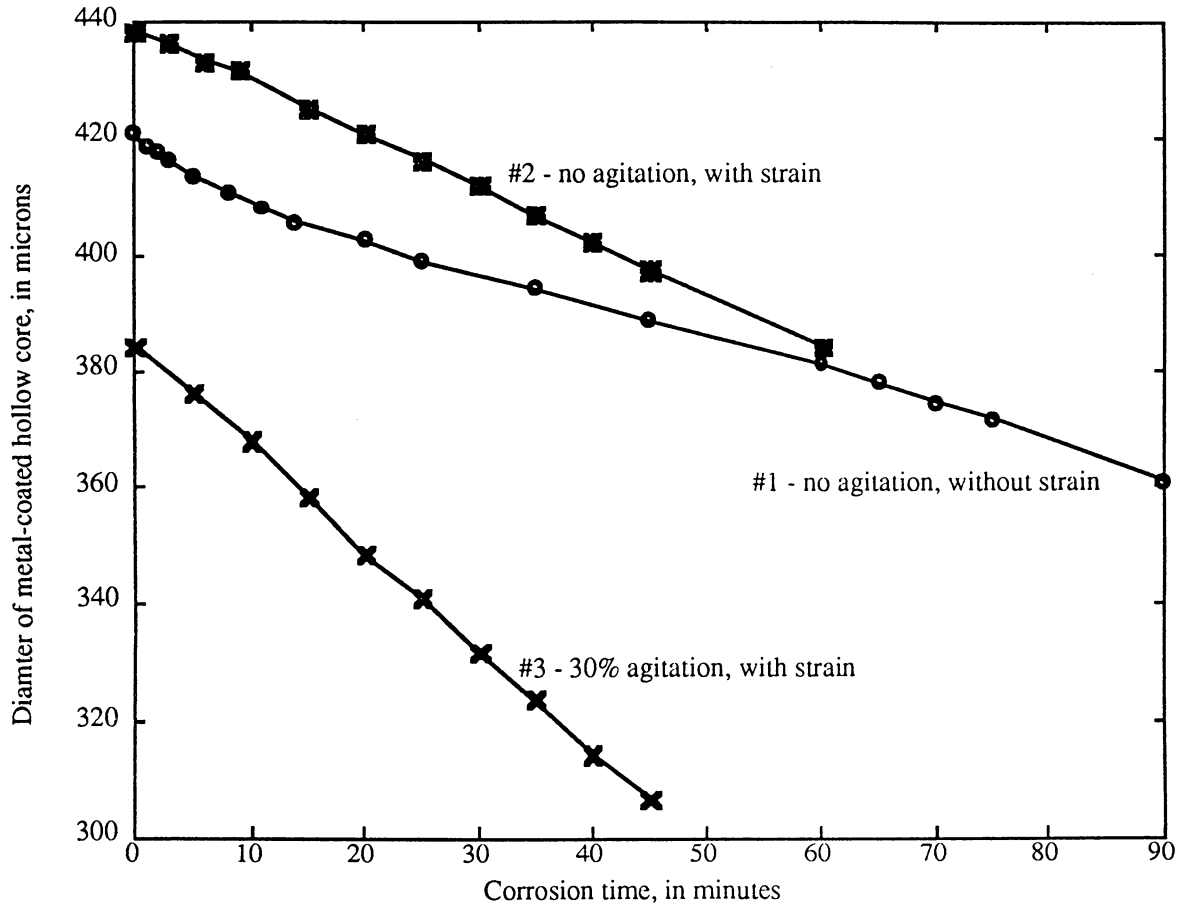

Figure 3.4: Results of corrosion rate tests

to be tested; however, one sensor broke while attempting to measure the thickness of copper on the hollow core with a set of mechanical micrometers. This method of measuring the coating thickness was later abandoned, for fear of breaking too many sensors. The three remaining sensors were then all corroded in an agitated solution, and from the fringe information and sensor gauge length, the strain release curves seen in Figure 3.5 were developed. Conflicting results exists for these three sensors; the sensor with the least amount of copper coating took the longest time to show a complete response. However, the third sensor showed the greatest amount of strain release, and was also the quickest to corrode. This follows since the copper coating would have been under more compressive strain, corroding faster due to stress corrosion. It should also be noted that the fringe contrast of the output signal (defined as the peak-to-peak voltage level of the EFPI output signal) in two of the three cases increased over the testing period, supporting the assertion that the sensor was relaxing during the tests, decreasing the gap size and increasing the fringe contrast. (Refer to Figure 2.2)

The next three sensors were tested in a similar fashion, except in a 10% agitated solution. The response was recorded on a digital sampling oscilloscope, and an attempt was made to store the traces for future use. Unfortunately, an acquisition error was made, and the traces were lost. No additional data is available for these tests, except that the output showed multiple fringes during the corrosion cycle, as expected.

The final four sensors were corroded in the same manner as the previous two, except more care was taken to acquire the data on the oscilloscope, and consequently none of the traces were lost. Since most of the fabrication, mounting and electroplating "bugs" were solved by the time these tests were performed, they resulted in being the most informative. The

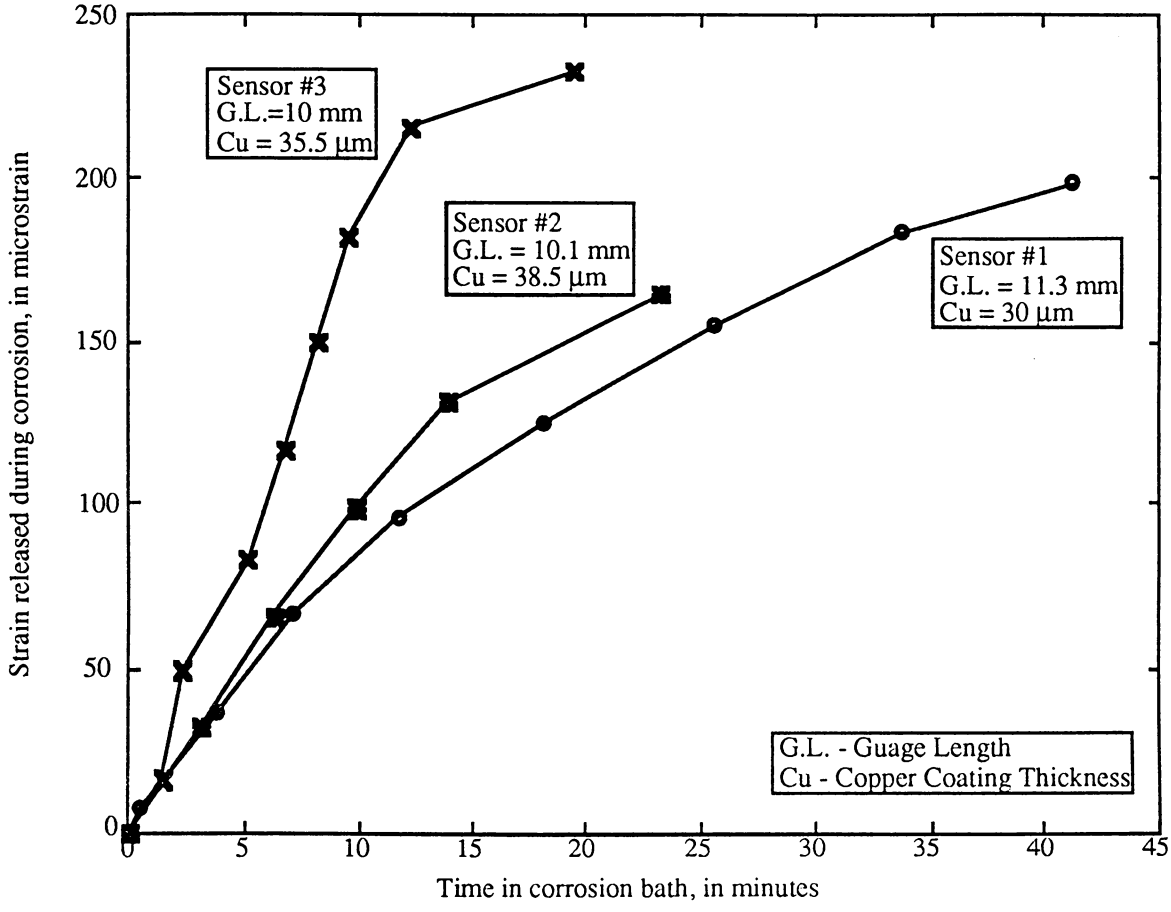

Figure 3.5: First EFPI corrosion sensor test results

remainder of the experimental discussion on the EFPI corrosion sensors will focus on this final series of tests.

3.4.2.1 Focus on EFPI Corrosion Sensor Test Results

The EFPI output traces are seen in Figures 3.6 and 3.7. All four of these sensors had approximately 50 microns of copper coating on the hollow core fiber. The differences in the number of interferometric fringes seen on the four sensors stems from two factors: the stainless steel rack used to pre-strain the sensors did not impart the same amount of strain on all the sensors, and also the gauge length for each sensor was different. Fifty microns was a sufficient amount of copper to hold the sensor in the strained position, despite the aforementioned challenges the stainless steel rack presented. To detach the sensors from the rack, a razor blade was carefully used to pop the epoxy bead off of the rack. In most cases, one of the glue beads was extremely easy to remove, and it was evident that plating solution had leaked past the StopOff®, and attacked the epoxy, since there was a small amount of copper that had plated onto the stainless steel rack *underneath* the epoxy bead. Also, there were some problems with the adhesion between the sensor fiber and the epoxy, but this loss of adhesion became negligible when the copper coating was removed from the polyimide-coated fiber; the adhesion between the copper coating and the polyimide is much worse than the adhesion between the polyimide and glass fiber.

An interesting phenomenon is observed in Figure 3.6 (a); first note that the initial eight minutes on the oscilloscope trace is not the response of the sensor to the corrosion bath, but to immersion in de-ionized water. This short test was conducted to observe the sensor's behavior to outside disturbances like liquid agitation, fume hood vibration, etc. Some drift occurred, but this is considered to be negligible. After eight minutes, the sensor was

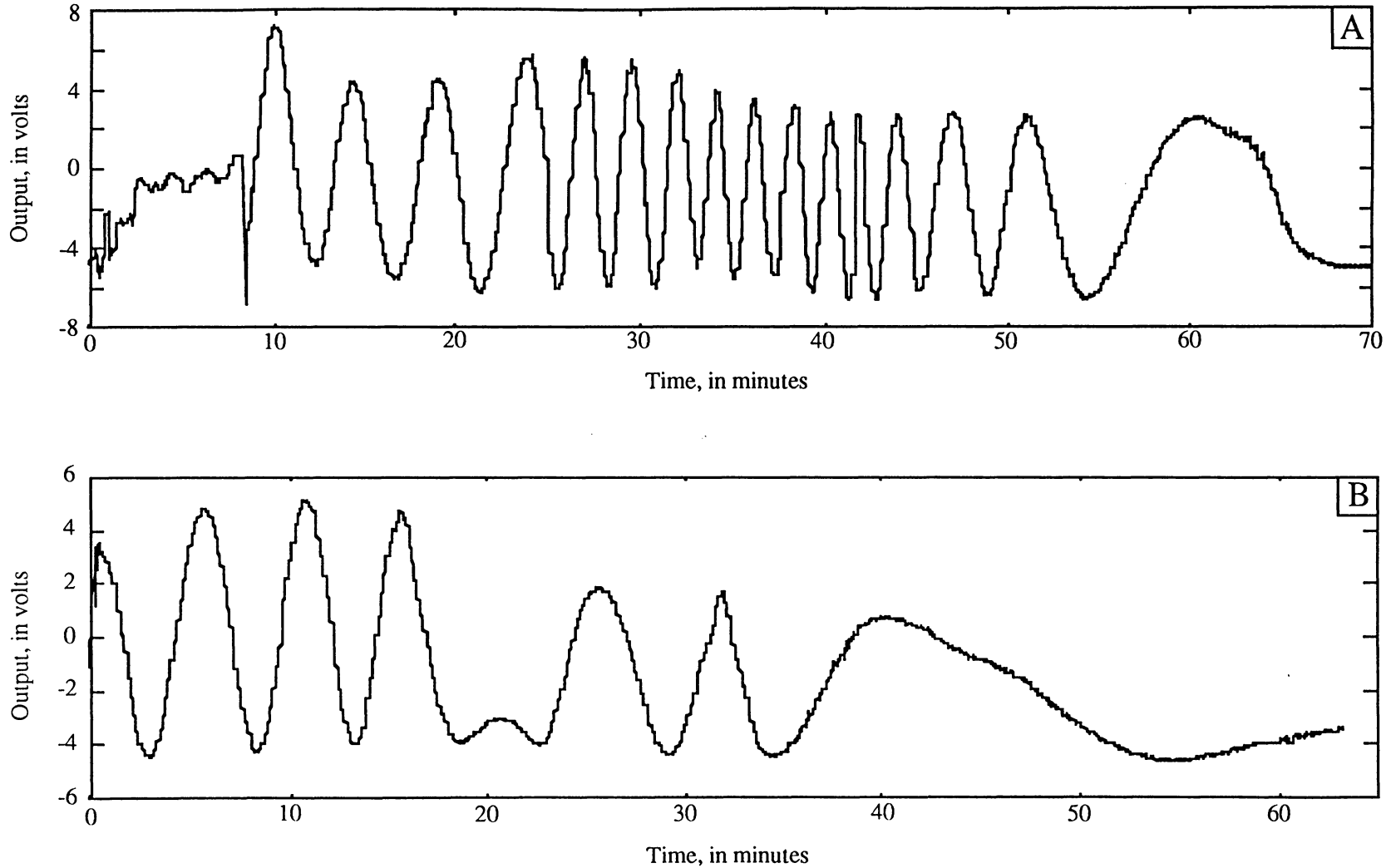

Figure 3.6 (a),(b): EFPI corrosion sensor test results

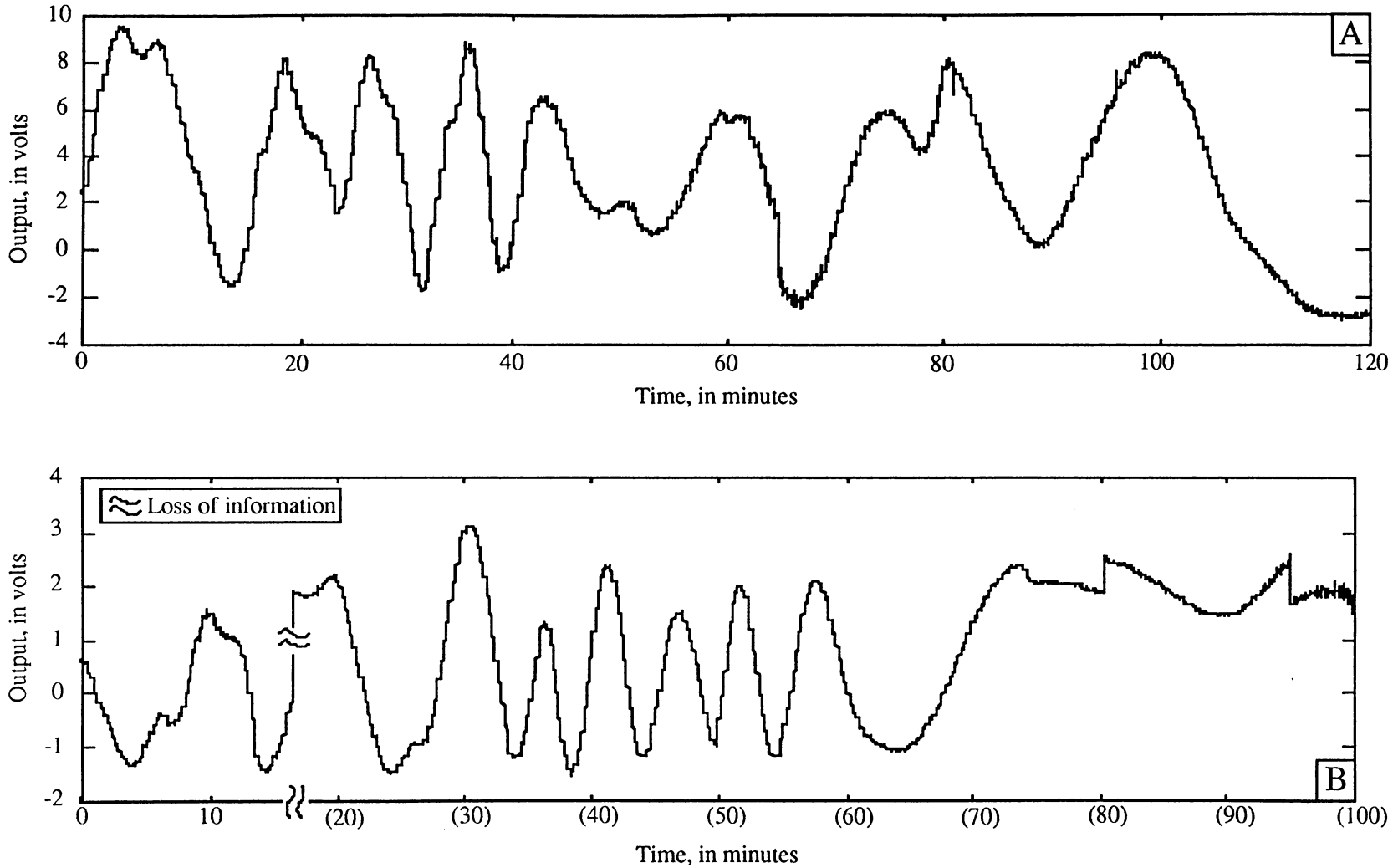

Figure 3.7 (a),(b): EFPI corrosion sensor test results

removed from the water and placed in the corrosion bath. Immediately, the sensor began to show a release of stored strain. Note that the rate of corrosion was slow at first (8-25 minutes) but then later increased as the coating of copper was removed (25-43 minutes). The reduction in the corrosion rate after 43 minutes is due to the fact that an insufficient amount of copper exists on the sensor to hold any more strain; although not pictured here, the oscilloscope trace remained at the same voltage level beyond 70 minutes. (This was true for the end of all the traces. Typically, the copper was completely removed during the last 5-10 minutes of the oscilloscope trace shown.)

Since the copper coating was applied as the sensor was relaxing (due to the aforementioned adhesion problems), the coating was under more compressive strain near the hollow core fiber than at the surface. It then follows that the rate of corrosion would be faster as the coating decreased, due to stress corrosion. Figure 3.6 (a) supports this hypothesis, evident from the increase in frequency of the oscilloscope fringes. Another contributing factor that could have caused an increased response rate is wicking of corrosion solution under the copper coating, causing a loss in adhesion at the metal/glass interface. It is not known if this in fact took place, but one piece of evidence exists to support this hypothesis. Following the corrosion experiments, the sensors were examined under a microscope. In more than one case, the copper was completely removed from one side of the hollow core fiber, while the other side maintained a very thin coating, suggesting there was a preferential rate of corrosion over the circumference of the cylindrical hollow core. This could have been caused by corrosive liquid wicking in through the end of the sensor, and traveling down underneath the copper coating to the hollow core. However, this hypothesis is not completely airtight; because the solution was being agitated, it is possible that the medium was impinging upon one side of the sensor with more force than on another. Since

insufficient evidence exists to support either of these ideas, it is unclear whether one, both, or neither of these factors caused a change in the sensor's response. What is not in question is that there is an increased rate of corrosion as the sensor loses its metal coating; by comparing the theoretical model to the actual data, for the same coating thickness and sensor parameters, it is apparent that the rate of corrosion is faster in the experimental results, as depicted in Figures 3.8, 3.9 and 3.10.

Figure 3.6 (b) does not exhibit the same increase in corrosion rate as Figure 3.6 (a), possibly because there are simply less fringes, an insufficient number to determine if there was an increase in the corrosion rate. More likely it is because there was simply not as much pre-strain on the EFPI sensor before plating, subduing the stress corrosion effect. This hypothesis is supported by examining each sensor's gauge length; since they both had comparable gauge lengths, they should exhibit a similar number of fringes for the same strain. An interesting phenomenon occurs after twenty minutes in the corrosion bath; there is either a change in the direction of the EFPI sensor, or turn-around point, or an extensive amount of loss in the output signal. There is no evidence to support the presumption that this is a turn-around point; there is a hypothesis, however, to support the premise that there was a loss in signal power. Recall that the EFPI sensors that were fabricated for these tests were made with 155 micron diameter polyimide single mode fiber, and 190 micron inner-diameter hollow core fiber. Hence there is 17.5 microns of leeway in either transverse direction for the single mode fiber to move around in; furthermore, the actual diameter of the single mode fiber with the polyimide coating removed is 125 microns, increasing the margin of mismatch between the fiber endfaces and the hollow core fiber to 32.5 microns in any direction. This lack of consolidation leads to alignment problems with the fiber endfaces; the more severe the misalignment, the less power that is received by the photodetector. The

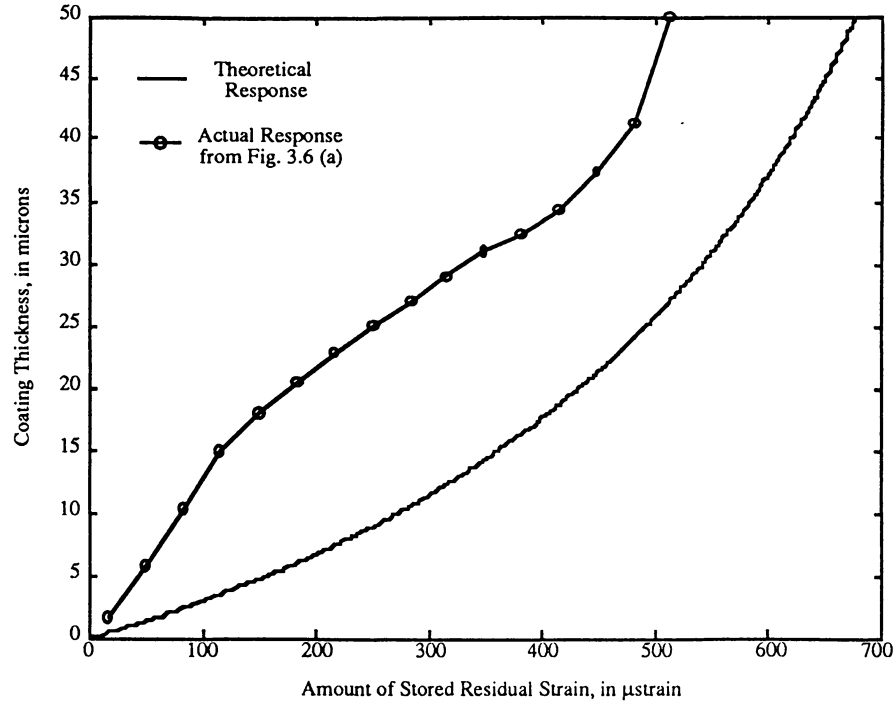

Figure 3.8: Theoretical and experimental EFPI test results for Figure 3.6 (a)

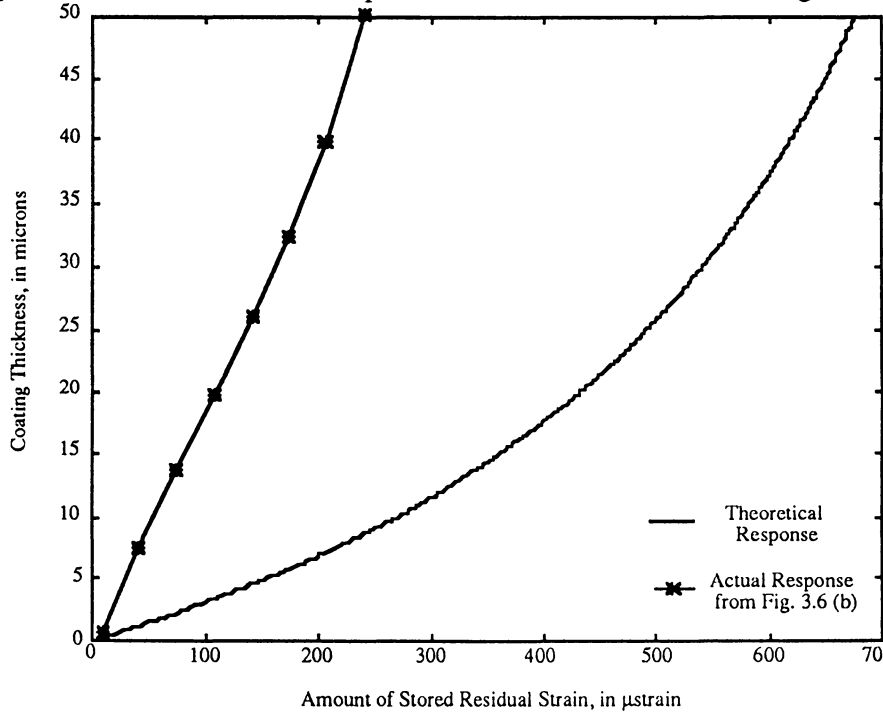

Figure 3.9: Theoretical and experimental EFPI test results for Figure 3.6 (b)

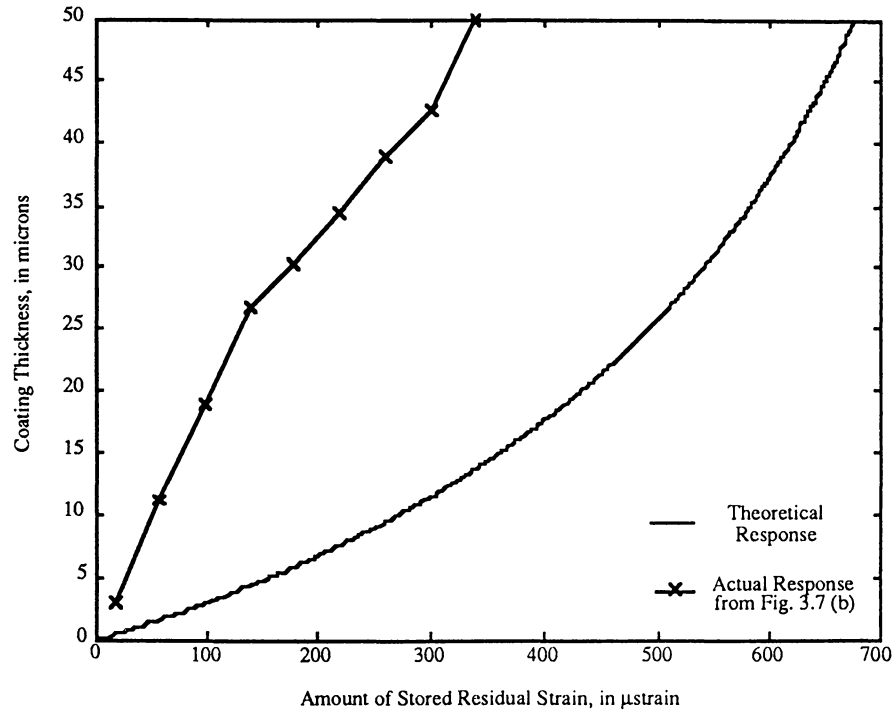

Figure 3.10: Theoretical and experimental EFPI corrosion test results for Figure 3.7 (b)

proposed explanation for a severe decrease in the signal power at 20 minutes on Figure 3.6 (b) is that, as the sensor is relaxing, it is also becoming misaligned. This change in the output power is much more pronounced in Figure 3.7 (a). Further problems could be encountered if the endfaces of the EFPI sensor are not cleaved at right angles, aggravating any angular misalignment problems[32]. The misalignment in either case could be produced from a nonuniform rate of corrosion over the surface of the sensor, or from local disbonding of the copper coating on the surface of the hollow core fiber. The latter is more probable, since the surface of the coated sensors was found not to be uniform, as previously envisioned. Evidence of this can be seen in Figure 3.11, two scanning electron microscope pictures of an electroplated sensor before corrosion; these photographs show irregularities on the surface of electroplated sensors. These uneven protrusions could cause a local change in the amount of stored strain, possibly sufficient to cause alignment problems. Finally, it should be noted that the loss of information in Figure 3.7 (b) causes the remainder of the data following the information gap to be somewhat misleading; the time axis is shown as being continuous, though the times would certainly be greater for a given point on the oscilloscope trace. The discontinuities seen after approximately 70 minutes were caused by factors outside of the corrosion bath, specifically, a change in the coherence of the splice tube used to unite the sensor to the EFPI support system, causing only a DC-shift in the voltage trace.

3.4.3 AEFPI Corrosion Sensor Test Results

Not as much success was encountered in using the absolute EFPI system for corrosion detection as was observed with the EFPI system. The principal reason for this was the absolute system's tendency to continually drift during acquisition; even after taking steps to stabilize the temporary splice between the sensor and the support system, the computer

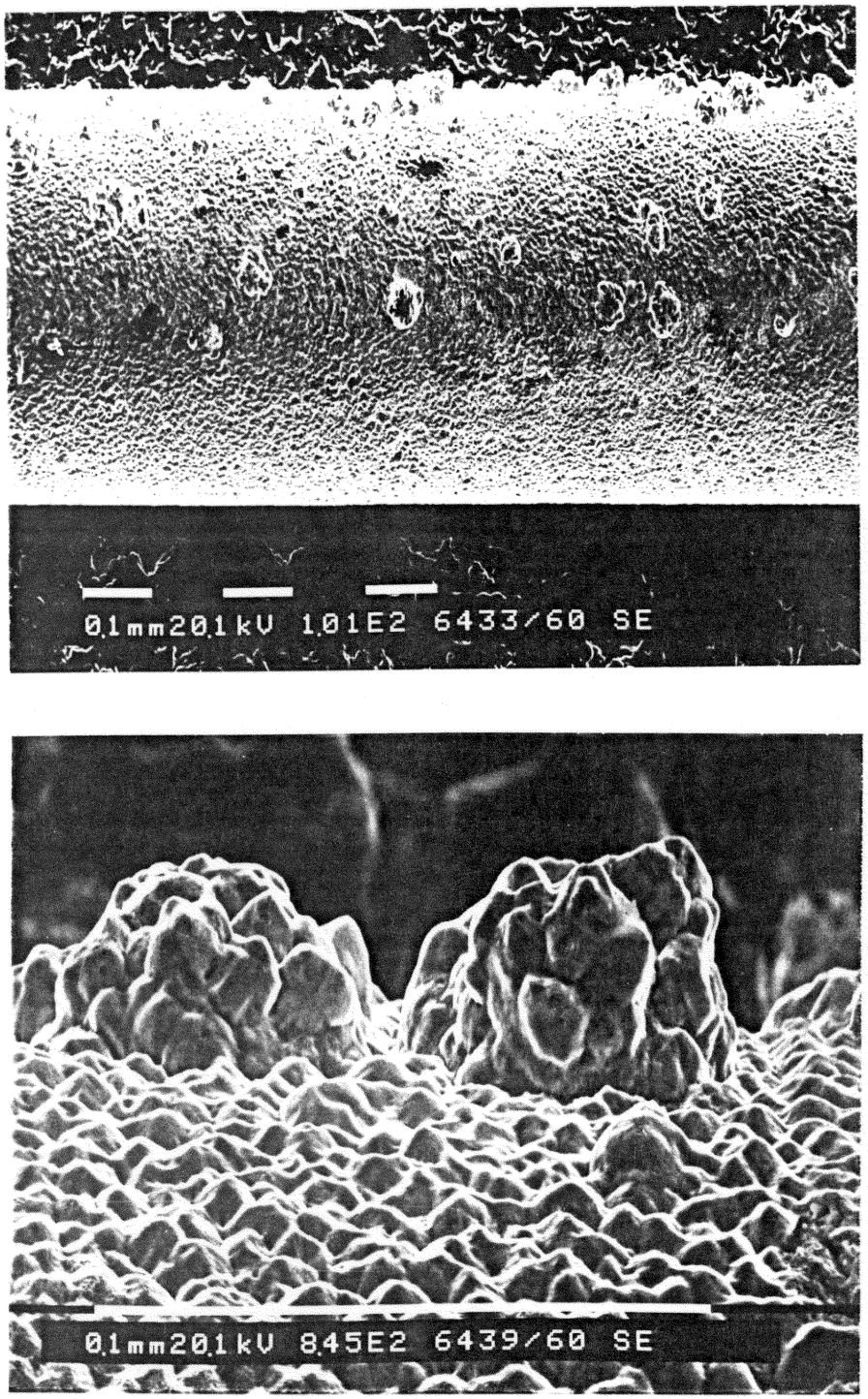

Figure 3.11: SEM photographs of copper coated strain sensor, before corrosion

read-out continued to fluctuate. The results for one successful test are shown in Figure 3.12. Although only one test is reported, several more were performed without promising results. On more than one occasion, the output signal of the absolute system simply remained at the same level, oscillating about one gap value. The reason more positive results were attained for the EFPI sensors and not the AEFPI sensors is that the EFPI is inherently more sensitive. Recall that one output fringe on the EFPI system translates into a perturbation of $\lambda/2$. For the 1330 nanometer wavelength system used, one fringe translates into a gap change of 665 nanometers. The resolution of the absolute system is one micron, but the errorbar is approximately 2 microns, at best. Hence, a minimum of about six fringes on an EFPI system would have to be stored in the sensor to observe a response. The one test that is reported for the AEFPI system was for a sensor that was pre-strained over 0.1% strain; further tests of this kind were not conducted, for fear of breaking too many sensors. Also, the adhesion problem discussed earlier would increase for higher strains, reducing the amount of time the sensor would be in strain. Recall that the deposition rate during electroplating is limited by the small area which is being plated, and its inability to maintain a high current density.

3.4 Corrosion of Metal Coated LPG Sensors

The LPG corrosion sensor measures the change in the index of refraction of the material surrounding the cladding when a metal coating is removed from the sensor. Hence, it was not necessary to take as many steps in preparing the sensors as with the EFPI and AEFPI strain sensors. Two LPG sensors were subjected to corrosion testing; one was tested once with an evaporated coating of copper, the other twice, first with an evaporated and electroplated coating of copper, second with an evaporated coating of nickel. Nickel does not corrode as readily in our corrosion bath; it was used primarily to show that the LPG

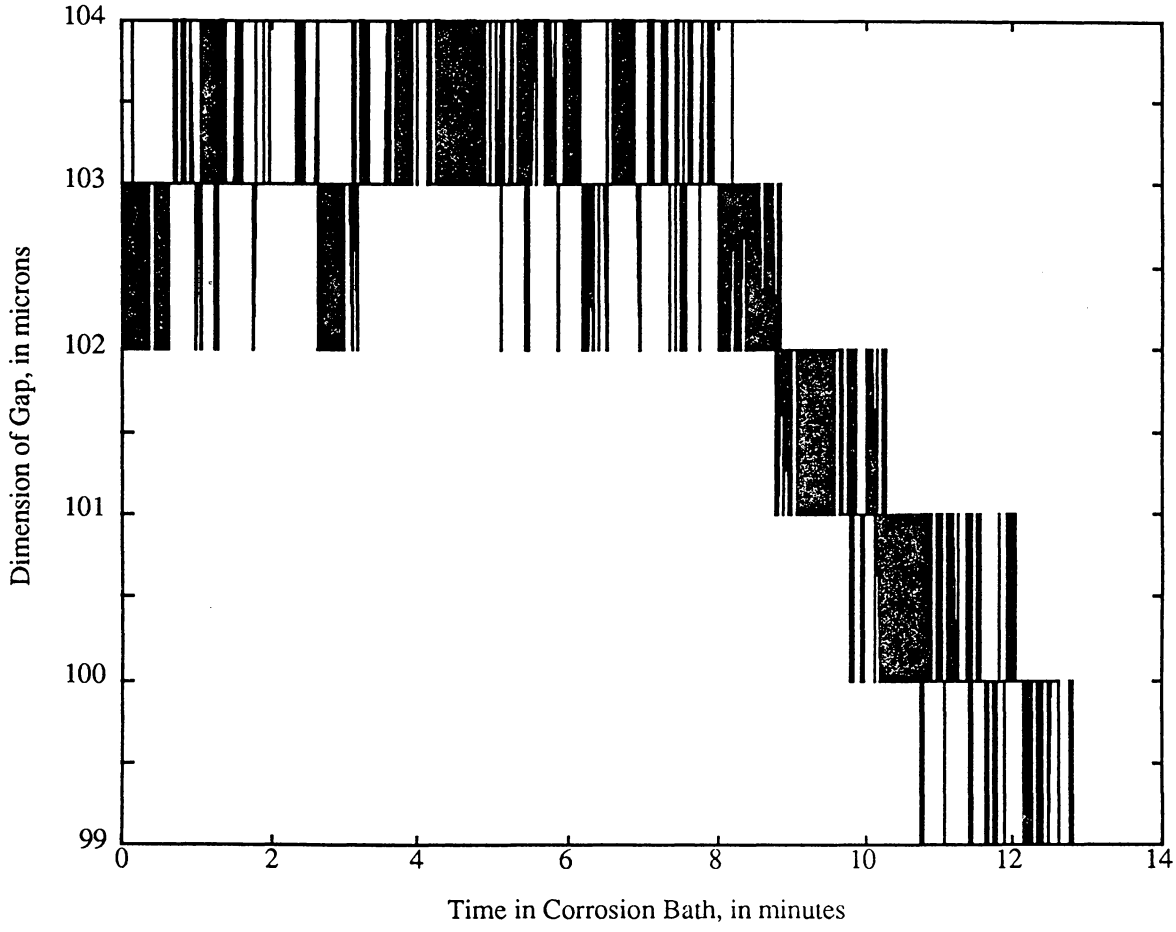

Figure 3.12: AEFPI corrosion sensor test results

corrosion sensor achieves results regardless of the metal used to coat the sensor. Because the interaction between the metal coating and evanescent cladding modes occurs only at the actual metal-glass boundary, it was not necessary to deposit very thick coatings of metal.

3.4.1 LPG Corrosion Sensor Test Results

The first test was with copper, and a thickness of fifteen microns was deposited. The sensor was then bonded to the stainless steel rack with Devcon® five minute epoxy. This was done only to ensure that the sensor remained in the straight position during the tests. Hardcopy traces were taken periodically throughout the tests; by overlapping the traces taken at the beginning and end of the tests, as shown in Figure 3.13, one can examine the attenuated wavelength shift. Since overlapping each trace would only confuse the issue, the results of the entire test are shown as in Figure 3.14. As the copper coating is removed, the LPG sensor is exposed to more of the corrosive medium, causing a change in the index of refraction at the cladding boundary, and hence causing the wavelength of the attenuated signal to shift. However, because the ambient medium changes from copper to the corrosion solution, the initial shift seen during corrosion is not of interest, since real-world situations would cause the sensor to be exposed to air, not the corrosion medium employed in this study. By removing the sensor from the medium after all the metal is corroded off and cleaning off any residual acid, the response of the sensor to air is determined, and compared to the response while coated with metal. Similar results are shown in Figures 3.15 and 3.16 for the other LPG sensor coated with copper, as well as the first sensor coated a second time with nickel. Comparing the two copper tests, note that although there was a thicker coating of copper on the first test, the time it took to remove all of the copper is less. As shown on the figures, the concentration of the corrosive solution was less for the

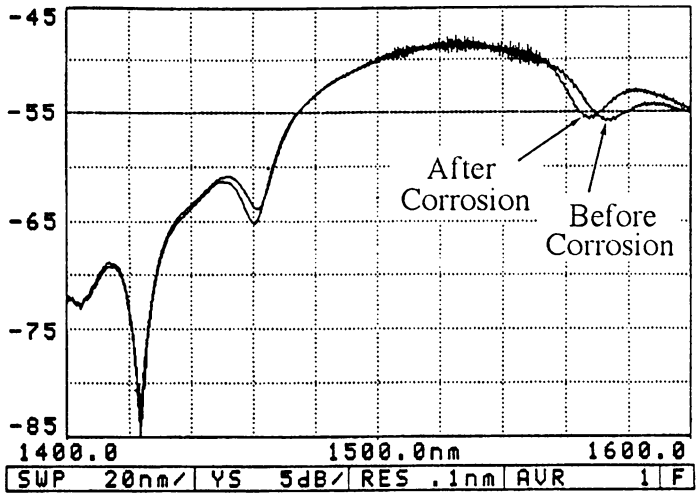

Figure 3.13: OSA traces of LPG corrosion test results

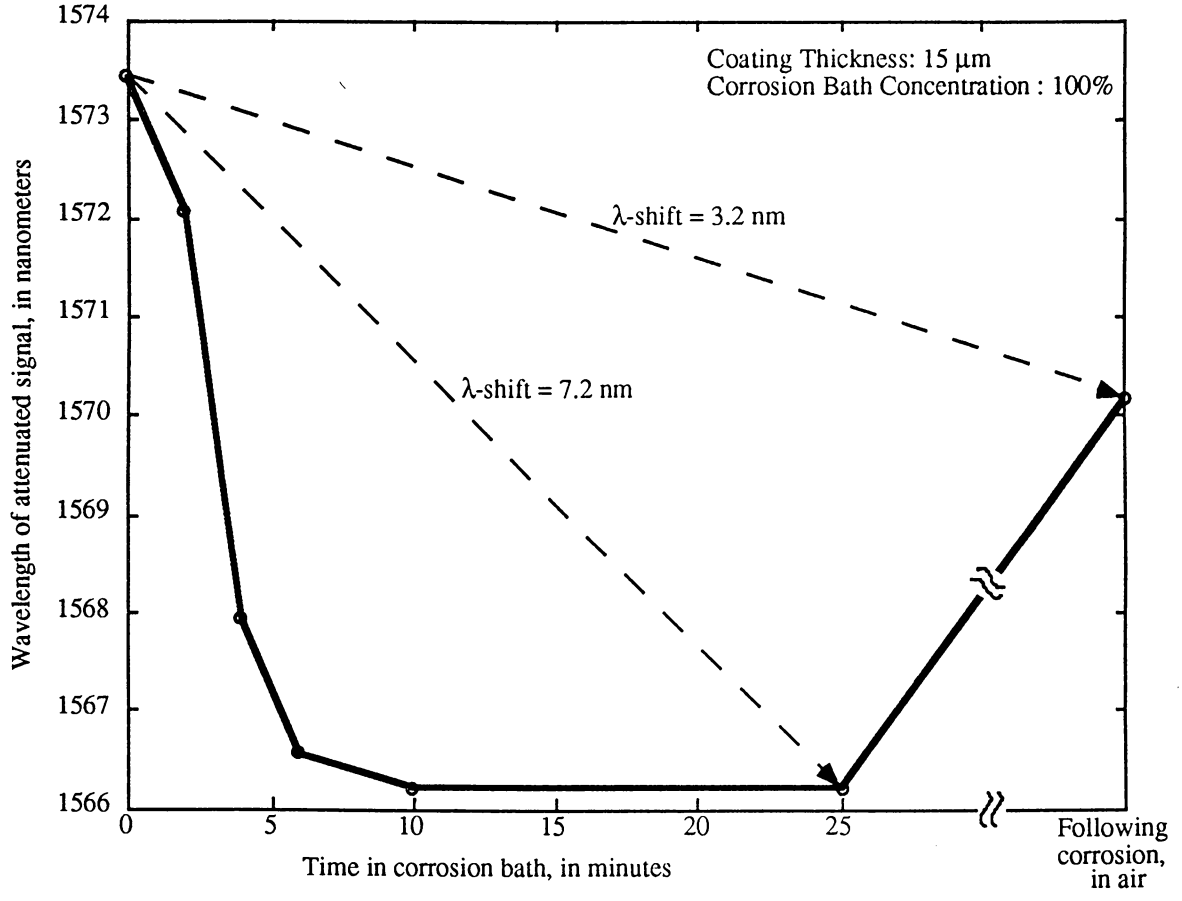

Figure 3.14: Overall results from LPG corrosion sensor test, copper coating

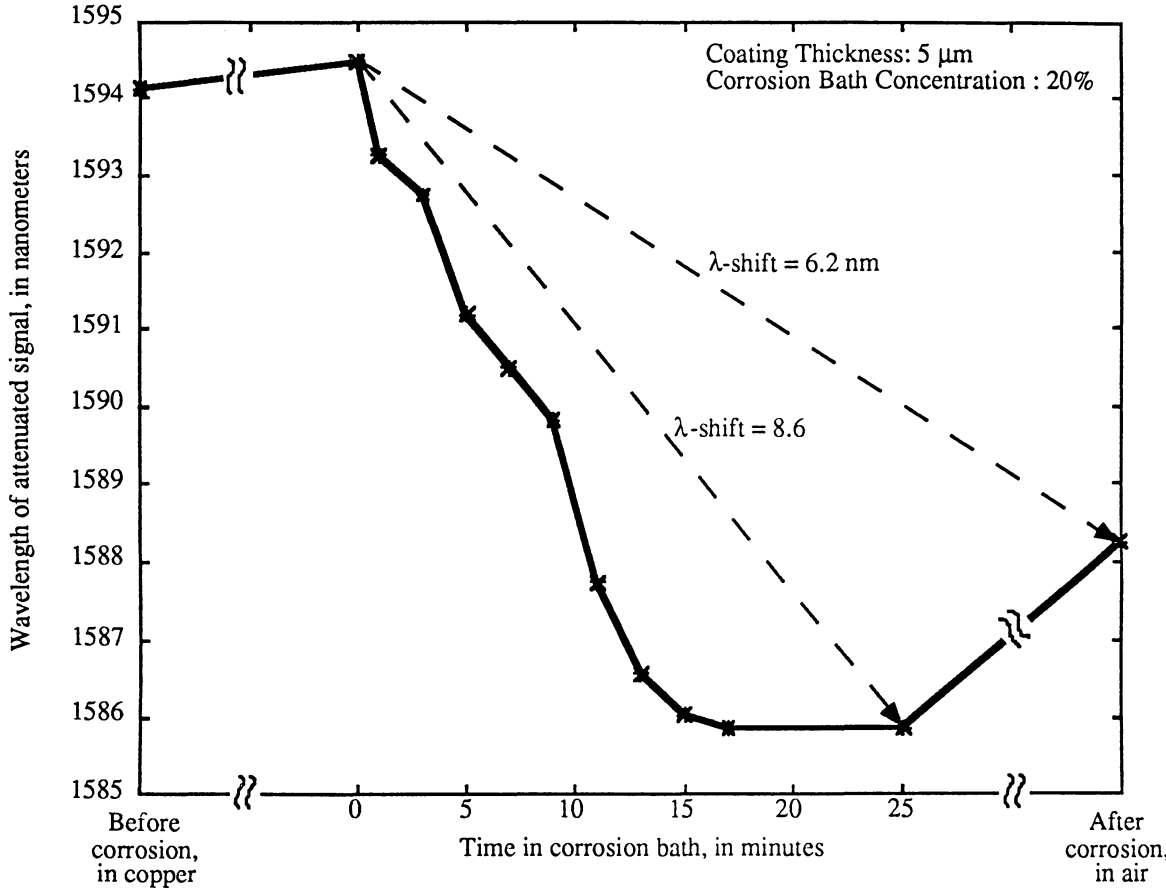

Figure 3.15: Overall results from LPG corrosion sensor test, copper coating

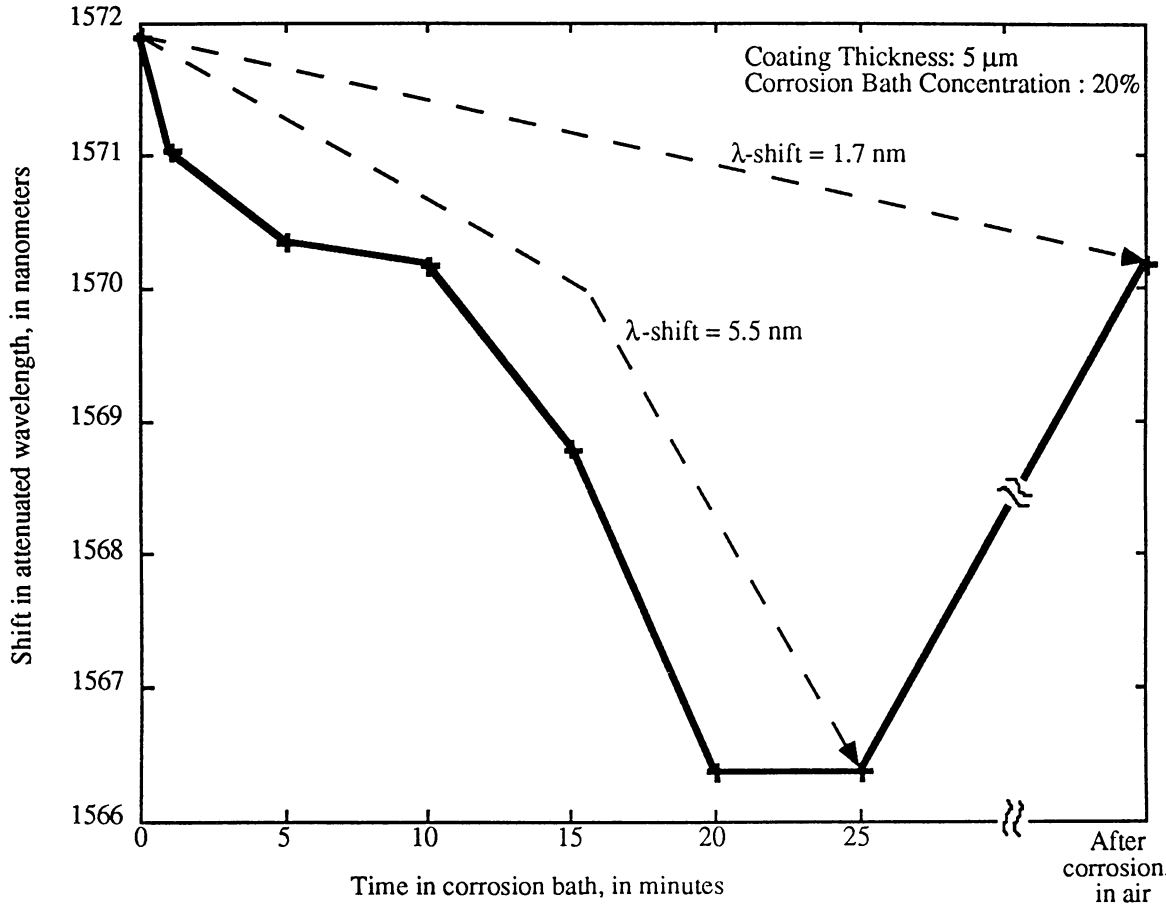

Figure 3.16: Overall results from LPG corrosion sensor test, nickel coating

second test; after performing the first test, subsequent tests were performed with a water-diluted corrosive solution, to slow the response time.

All three tests showed that when the LPG sensor is coated with a metal, there is an increase in the wavelength of the attenuated signal. As the metal is removed, the wavelength of the attenuated signal decreases, the minimum amount being 1.7 nanometers. This wavelength shift is a discernible amount of change for standard methods of interrogation, such as with an optical spectrum analyzer or monochrometer. Some other experimental data[33] collected by researchers at the Fiber & Electro•Optics Research Center, shows the typical response of an LPG fiber sensor to different indices of refraction. The results of this test are shown in Figure 3.17. To properly interpret this graph, it should be noted that, as the index of refraction approaches that of the fiber, the output magnitude of the attenuated wavelength decreases; hence the data points around an index of refraction equal to 1.55 contain a large amount of error. The index of copper is much greater than that of glass, and the index of refraction of the corrosion solution is approximately 1.4. Hence, our tests correlate well with those obtained in the refractive index tests; the only point of debate is whether the response of the LPG sensors was on the left or right side of 1.45 in Figure 3.17 during exposure to the corrosion bath. Based on the data obtained during corrosion, it is reasonable to assume that the response of the LPG sensor in the corrosive medium corresponds to the right side of 1.45, since the peak attenuated signal did not experience a minimum value during the corrosion tests. Since the sensor was removed very quickly from the corrosion bath and exposed to air, the response moved through the minimum value at an index of 1.45, to the value of 1.0 for air.

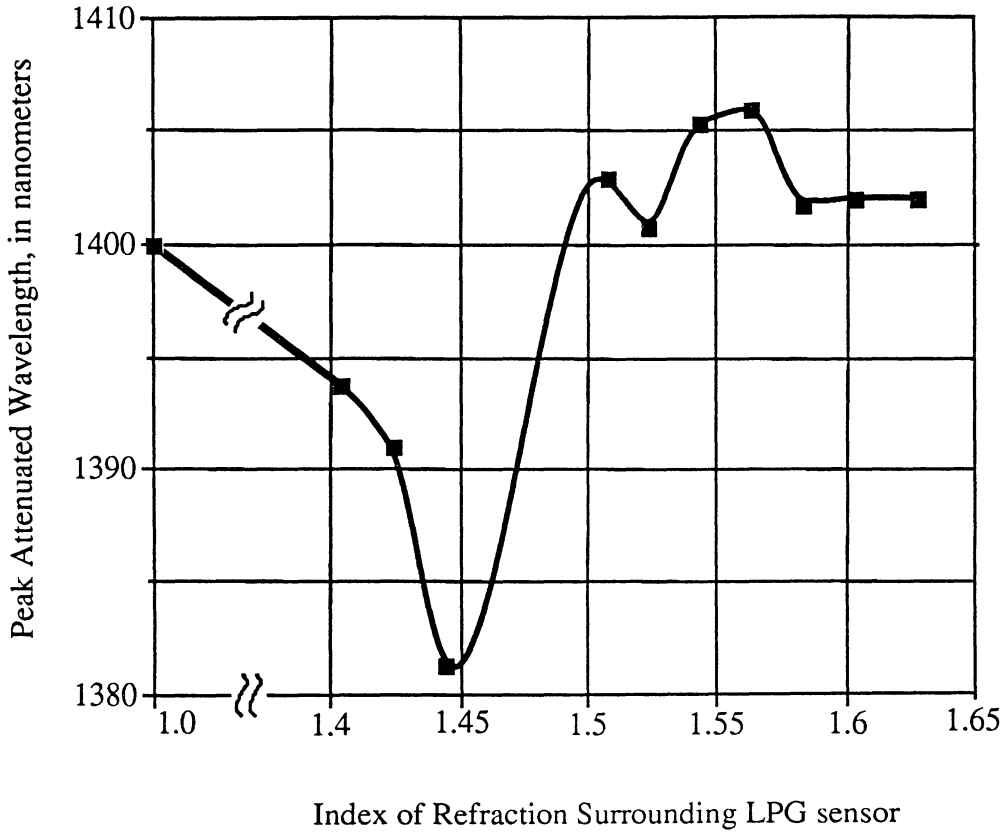

Figure 3.17: LPG sensor response to different indices of refraction

Chapter Four - Conclusion

This thesis study was successful in demonstrating a method of corrosion detection through the reduction in mass of a metal coating on the surface of fiber optic sensors. Two principal corrosion monitoring techniques were employed, one based on the ability of a thick metal coating to maintain residual strain in a fiber optic strain sensor, namely the extrinsic Fabry-Perot interferometer, the other based on the change in the index of refraction a coating of metal imparts upon the cladding region of a long period grating fiber optic sensor. Tests were performed on both the EFPI and AEFPI systems, with reliable results only with the EFPI system. Results for the AEFPI were inadequate to assert that the corrosion detection design is compatible with the system; however, should improvements be made in the future either to the AEFPI support system, or to the method of loading strain in the sensors, the system should work well for corrosion detection. Several points for improving strain sensor loading include:

- Redesign sensor strain rack to eliminate problem of sensor relaxation during the plating phase. Some ideas include to make the ends on the rack cylindrical, instead of rectangular, so that the lead in fiber and reflector fiber of the strain sensors can be wrapped around several times, using friction and possibly a small amount of adhesive to hold the sensors during straining.
- Improve upon the current method of applying strain; the single threaded bolt on the stainless steel rack does not apply even strain across several sensors at this time. One idea is to employ two smaller threaded pieces, to replace the current smooth bolts on which the sliding piece moves.

- In construction of the sensors, as well as that used to hold the sensors on the rack, utilize an adhesive that is not attacked by the acids found in plating solutions. The MS-907 epoxy is susceptible to acid attack, and will disbond or weaken.

Upon solving the adhesion problems encountered in this study, more metal can then be applied for a given amount of pre-strain. It is expected that this would then result in a sensor with more residual strain storage, giving a greater response, as well as making the AEFPI system feasible as a candidate for corrosion monitoring.

Another important detail that should be restated is the need to test this technology using more traditional corrosion testing techniques; these include salt-spray tests, or fog tests, as described in ASTM procedures[34]. These types of tests are more acceptable for corrosion testing because they better model actual atmospheric conditions that are found in practical environments. Several interesting facets of corrosion are present in these tests that were absent from this study. They include (1) the response of LPG sensors as the thin coating of metal simply oxidizes, before any reduction in material mass occurs, (2) the affect corrosion by-products have on the strain response of EFPI or AEFPI sensors, and whether or not relaxation would occur at all, and (3) the response of either type of sensor when mounted on a surface undergoing corrosion, possibly including non-uniform corrosion over the surface of the sensor. As discussed in the Chapter One of this thesis, one might question the value of demonstrating corrosion sensing for copper, when most of the interest in corrosion detection (at least for the sponsors of this research) is in aluminum. This preliminary study was specifically designed to produce a metal corrosion sensor; copper was simply the easiest metal to deposit on the surface of the sensor, as well as to electroplate. Aluminum develops an insulating oxide layer very quickly, making electroplating extremely difficult. Should future research be conducted on this subject, one

of two courses of action seem required; either perform the same kinds of tests on aluminum coated sensors, examining additional characteristics of corrosion that might not be present in copper, or continue examining ways to implement aluminum corrosion detection with copper coated (or another metal) sensors, and attempt to correlate sensor response to the corrosion parameters of aluminum. This method could be possible as more advancements in sensor architecture develop or different metal deposition ideas evolve. It is more likely, though, that the most feasible way would be to master the methods of depositing thick coatings of aluminum on the sensors, to effectively interrogate aluminum corrosion.

References

1. S.K. Chawla, T. Anguish, J.H. Payer, "Microsensors for Corrosion Control," *Materials Performance,* Vol. 20, No. 5, pp. 69-74, May 1990.

2. A.S. Brown, "Industry Seeks Tonic for Aging Aircraft," *Aerospace America*, Vol. 30, no. 3, pp. 24-28, March 1992.

3. Tour of USAir Maintenance Facilities, Roanoke Regional Airport (Woodrum Field), Roanoke, Virginia, October, 1993.

4. J.A. von Fraunhofer, Concise Corrosion Science, Portcullis Press Ltd., London, 1974.

5. W.H. Ailor, Handbook on Corrosion Testing and Evaluation, John Wiley & Sons, New York, 1971.

6. W.L. White, H. Leidheiser Jr., "The Corrosion Coulometer - A New Corrosion Monitor for Steel Structures," Corrosion, Vol. 46, No. 8, pp. 653-661, August 1990.

7. G.K.Brown, N. Rothwell, "Corrosion Surveillance for Continuous Pipeline Integrity Monitoring," *Corrosion Prevention & Control,* Vol. 40, No. 1, pp. 19-23, February 1993.

8. A. Legat, C. Zevnik, "The Electrochemical Noise of Mild and Stainless Steel in Various Water Solutions," *Corrosion Science,* Vol. 35, No. 5-8, pt. 2, pp. 1661-1663, 1993.

9. J.H. Payer, "Controlling Corrosion in the Process Industries," *Sensors*, pp. 8-16, Vol. 7, No. 4, April 1990.

10. W.H. Smyrl, M.A. Butler, "Corrosion Sensors," Interface, The Electrochemical Society, Vol. 2, No. 4, pp. 35-39, Winter 1993.

11. A. Chase, ""Real -Time" Monitoring of Contact Corrosion for Process Control Systems," 78th Annual Meeting of the Technical Section of the Canadian Pulp and Paper Association, Montréal, Québec, pp. 189-193, January 28 and 29, 1992.

12. J.M. Galbraith, "In-Service Corrosion Monitoring with Automated Ultrasonic Testing Systems," The International Arctic Technology Conference, The Society of Petroleum Engineers, pp. 341-347, Anchorage, May 29-31, 1991.

13. H. Goedecke, "Corrosion Surveys with the *UltraScan* Pig," *Corrosion Prevention & Control,* Vol. 37, No. 2, pp. 33-36, April 1990.

14. Z. Szklarska-Smialowska, R. Krishnakumar, "Ellipsometry in Studies of Metallic Corrosion and Oxidation," M.G.S. Ferreira, C.A. Melendres, (Ed.), Electrochemical and Optical Techniques for the Study and Monitoring of Metallic Corrosion, Kluwer Academic Publishers, Dordrecht, 1991.

15. P. Heimgartner, J. Weber, "Thin-Layer Activation for Detecting Minute Losses of Material due to Corrosion or Wear," Sulzer Technical Review, pp. 20-22, Vol. 72, No. 1, 1990.

16. W.J.H. Bender, A Chemical Sensor Based on Surface Plasmon Resonance on Surface Modified Optical Fibers, Doctor of Philosophy Dissertation,. Department of Chemistry, Virginia Polytechnic Institute and State University, 1992.

17. M. Miller, Optical Fiber-Based Corrosion Sensor Systems, Doctor of Philosophy Dissertation, The Bradley Department of Electrical Engineering, Virginia Polytechnic Institute and State University, 1995.

18. M.R. Sajan, T.S. Radha, B.S. Ramprasad, "Measurement of the Corrosion Rate of Aluminum in Sodium Hydroxide Using Holographic Interferometry," Optics and Lasers in Engineering, pp. 183-188, Vol. 15, 1991.

19. P. Jernberg, "Corrosion Evaluation of Coated Sheet Metal by means of Thermography and Image Analysis," *Thermosense XIII,* SPIE Vol. 1467, pp. 295-302, 1991.

20. J.S. Namkung, M. Hoke, R.S. Rogowski, S. Albin, "Detection of Aluminum Corrosion by Evanescent Wave Absorption Spectroscopy With Optical Fibers," Smart Structures and Materials Conference, San Diego, September 1995.

21. S.H. Poland, Applications of Optical Fiber Sensors with Thick Metal Coatings, Master of Science Thesis, The Bradley Department of Electrical Engineering, Virginia Polytechnic Institute and State University, May 1994.

22. K.A. Murphy, M.F. Gunther, A.M. Vengsarkar, R.O. Claus, "Quadrature phase-shifted, extrinsic Fabry-Perot optical fiber sensors," *Optics Letters*, Vol. 16, pp. 273-275, 1991.

23. V. Bhatia, Signal Processing Techniques for Optical Fiber Sensors Using White Light Interferometry, Master of Science Thesis, The Bradley Department of Electrical Engineering, Virginia Polytechnic Institute and State University, pp. 15-18, September 1993.

24. F.P. Beer, E.R. Johnston, Jr., Mechanics of materials, 2nd ed., McGraw-Hill, Inc., New York, 1992.

25. R.G. Budynas, Advanced Strength and Applied Stress Analysis, McGraw-Hill, Inc., New York, 1977.

26. R. Kashyap, "Photosensitive Optical Fibers: Devices and Applications," *Optical Fiber Technology*, Vol. 1, pp. 17-34, 1994.

27. A.M. Vengsarkar, P.J. Lemaire, J.B. Judkins, V. Bhatia, J.E.Sipe, and T. Erdogan, "Long-Period Fiber Gratings as Filters and Spectral Shape-Shifters," Post-deadline paper, *Optical Fiber Communications Conference*, San Diego, California, February 1995.

28. V. Bhatia, personal correspondence, April 25, 1995.

29. G. Keiser, Optical Fiber Communications, McGraw-Hill, Inc., New York, 1991.

30. J. Zeakes, Extrinsic Fabry-Perot Interferometric Hydrogen Gas Sensor, Master of Science Thesis, The Bradley Department of Electrical Engineering, Virginia Polytechnic Institute and State University, 1994.

31. Specifications Sheet, MS-907 epoxy, Miller-Stephenson, George Washington Highway, Danbury, Connecticut, 06810, (203) 743-4447, April 1995.

32. M.J.C. de Vries, Optical Fiber Sensors for Advanced Civil Structures, Doctor of Philosophy Dissertation, The Bradley Department of Electrical Engineering, Virginia Polytechnic Institute and State University, 1995.

33. Fiber and Electro•Optics Research Center, Data from LPG test performed by Mary Burford, April 15, 1995.

34. American Society for Testing and Materials, Annual Book of ASTM Standards, Vol. 03.02 "Wear and Erosion; Metal Corrosion," 1992.

The vita has been removed from the scanned document